Minimization of DC link capacitance in transportation application

by

Cristina González Moral

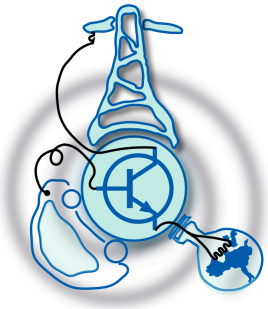

Submitted to the Department of Electrical Engineering, Electronics, Computers and Systems
in partial fulfillment of the requirements for the degree of

Master Course in Electric Energy Conversion And Power Systems

at the

UNIVERSIDAD DE OVIEDO

July 2016

Author .....

Certified by .....
Juan Manuel Guerrero Muñoz
Associate Professor
Thesis Supervisor

Minimization of DC link capacitance in transportation application

by

Cristina González Moral

Submitted to the Department of Electrical Engineering, Electronics, Computers and Systems
on July 22, 2016, in partial fulfillment of the
requirements for the degree of
Master Course in Electric Energy Conversion And Power Systems

Abstract

The DC-link capacitor is a bulky and expensive component. Therefore, there is an interest in reducing its capacitance in order to reduce both cost and size. An appropriate converter control can lead to a reduction of this component. In this thesis, the state of the art regarding capacitor reduction in the DC-link is analysed and classified according to the type of method employed. A general simulation is presented and analysed including all the components that conform the power electronics stage of a real scheme for vehicle hybridization. Using that scheme, some reduction methods are carried out and compared with the base case.

Keywords: DC-link capacitor reduction, control, feedforward, lifetime improvement, cost reduction, PMSM, PWM inverter, PWM rectifier.

Thesis Supervisor: Juan Manuel Guerrero Muñoz
Title: Associate Professor

Acknowledgments

Mis primeros agradecimientos son para el tutor de esta tesis de máster, Juanma, por su enorme comprensión en los duros meses que han acompañado a su realización. Por supuesto, por toda la ayuda prestada cuando quizá mi rendimiento no ha estado a la altura de lo que cabría esperar. Agradecimiento que extiendo a David Reigosa y Fernando Briz porque tuvieron ambos un comportamiento de lo más humano. Agradezco también a Christian Blanco y a Daniel Fernández por resolver mis dudas con Matlab y ayudarme cuando me tuve que enfrentar al "folio en blanco" inicial.

Uno de los mayores agradecimientos va por supuesto para Alejandro, que ha sido lo mejor de estos años y con la persona que más me he desahogado cuando las cosas no salían como esperaba. Tanto él como sus padres y familiares han sido un gran apoyo y lo valoro enormemente.

Agradezco en general a todos aquellos amigos que se han interesado por mí y me han animado, no solo durante este semestre sino durante los dos años que ha durado el máster.

Por último, agradezco a mi familia. A mi hermana Inés porque con su charla intrascendente me ayuda a desconectar del mundo. A mi madre Ana porque es la mujer más fuerte que conozco y sé que va a superar cualquier obstáculo que se le ponga por delante. A todos mis tíos, abuelos y primos porque siempre están cuando les necesito. Mención especial para Flecha, mi gran compañera y la única que jamás me juzgará siempre que le de comida dos veces al día. Finalmente, y como no podía ser de otra manera, esta tesis va dedicada a él, el mejor padre del mundo. Sé que nos has querido muchísimo y tu recuerdo me acompañará siempre. Aprendí tantas cosas de ti que no podrían escribirse ni en mil libros. Te quiero y te echo de menos.

Contents

List of Figures

List of Tables

Glosary

Acronyms

EV	Electric vehicle
HEV	Hybrid Electric Vehicle
PHEV	Plug in Hybrid Electric Vehicle
DC	Direct Current
AC	Alternating current
PMSM	Permanent Magnet Synchronous Machine
IPMSM	Interior Permanent Magnet Synchronous Machine
R	Resistance
L	Inductance
C	Capacitance
ESR	Equivalent Series Resistance
ESL	Equivalent Series Inductance
PWM	Pulse-Width Modulation
SVPWM	Space Vector Pulse-Width Modulation
P	Proportional Gain
I	Integral Gain
D	Derivative Gain
DPF	Displacement Power Factor
THD	Total Harmonic Distortion
AFE	Active Front End
VSI	Voltage Source Inverter
BEMF	Back Electromotive Force
RMS	Root mean square
PLL	Phase-Locked Loop
CAN	Controller Area Network

Variables

x_{qds}	Stator Complex variable
V_{abc}	Voltage in abc coordinates
i_{abc}	Current in abc coordinates
R_s	Stator phase resistance
λ	Flux linkage
v_x^s	Stator voltage in axis x
i_x^s	Stator current in axis x
ω_e	Electrical speed
ω_r	Rotor speed
P	Pole pairs in an electric machine or active power
Q	Reactive power
S	Apparent power
L_d and L_q	dq stator inductances
λ_{PM}	Permanent magnet flux linkage

Chapter 1

Introduction

Electric Vehicles (EV) / Hybrid Electric Vehicles (HEV) / Plug in Electric Vehicles (PHEV) are gaining popularity over recent years. The three of them have similar performance when powered only from the electric motor (short distances), but HEV/PHEV solves the problem for long distances (mainly having to wait for the battery to be recharged each 100 km more or less) thanks to having a conventional petrol engine that can be refuel as in a typical car. The main reasons to consider them as a option are listed below:

- **Disappearance of fossil fuels:** According to BP, one of the world's leading integrated oil and gas companies, there were proven oil reserves of 1700.1 billion barrels by the end of 2014, a 24% (330 billion barrels) increased over the last decade, enough to cover 52.5 years of global production. This means that every day there should be a consumption of 88720 million barrels [1]. If alternative energies are researched, these 52.5 years could be increased and the fuel used for those applications were it is still mandatory because there are no substitutes.

- **Independence of fossil fuels:** Reserves to production ratio (R/P) shows the remaining amount of a non-renewable resource, expressed in time. This ratio is show for petroleum in fig. 1-1 for 2014 and different regions.

  OPEC countries (Organization of the Petroleum Exporting Countries), hold the majority of the world's reserves, 71.6% of the global total. These countries are

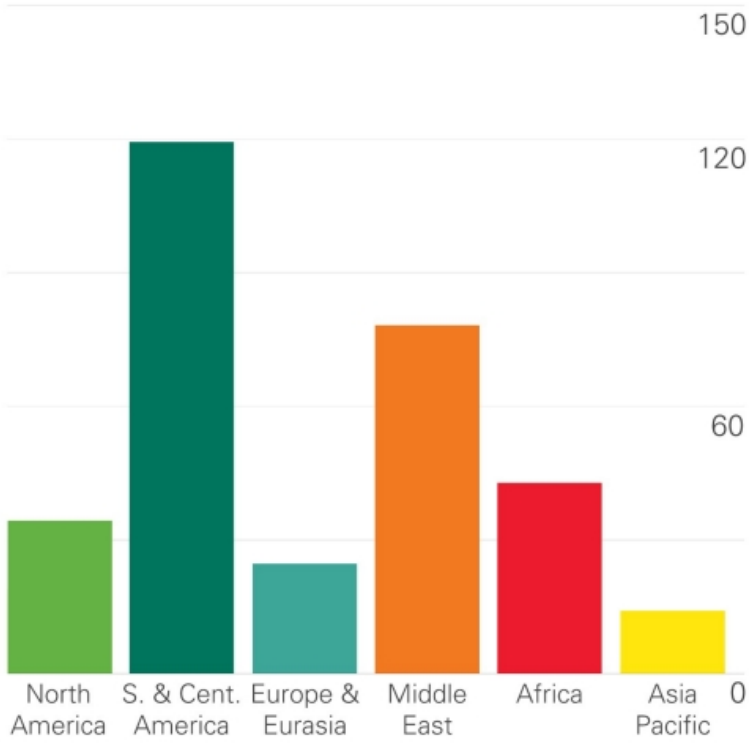

Figure 1-1: Reserves-to-production (R/P) ratios of petroleum in 2014 by region (years) [1].

13: Islamic Republic of Iran, Iraq, Kuwait, Saudi Arabia, Venezuela, Qatar, Indonesia, Libya, the United Arab Emirates, Algeria, Nigeria, Ecuador and Angola. South Central America holds the highest R/P ratio, more than 100 years [1].

As it has been shown, resources and consumption are not even. It is expected that, as reserves dwindle, this imbalance will cause prices to rise by countries that own more raw material. The situation could also lead to national security concerns, given the amount of things (not only cars) that are petrol-dependant in our society. These reasons, among others, triggered the search of alternative vehicles not powered from petrol, as electricity or hydrogen.

- **Pollution and global warming:** Recently, Earth's surface temperature has experience an increase in the global average temperature, as seen from fig. 1-2. The projection is that it will continue raising over the next hundred years, from

0.5 to 8.6^{o}C depending on the actions carried out to stop it [2].

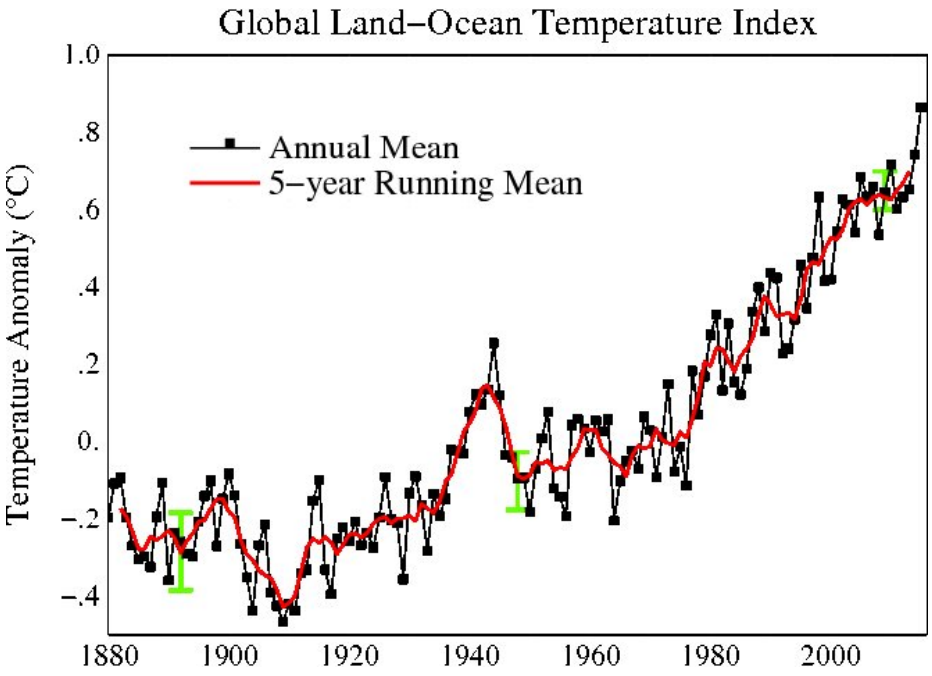

Figure 1-2: Global Annual Mean Surface Air Temperature Changes [3].

This change, as it may sound small, can cause large and dangerous shifts in both weather and climate. It is known as global warming, primary caused by an increased in the concentration of greenhouse gases in the atmosphere, the most important ones being carbon dioxide, methane, nitrous oxide and fluorinated gases. Among these gases, only carbon dioxide and nitrous oxide are produced in transportation.

Carbon dioxide (CO_2) has been traditionally the most worrying gas, and the one which governments and institutions have tried harder to diminish. CO_2 is the primary greenhouse gas emitted through human activities (80.9% of all US greenhouse gas emissions). Humans alter the carbon cycle because they add more to the atmosphere than the quantity naturally presented, at the same time cutting down forests that could absorb this excess back. 31% of all this gas comes directly from transportation activities, due to combustion of fossil fuels. Nitrous Oxide (N_2O) is also emitted in transportation (4% of all this gas emissions) when fuels are burned. The exact quantity depends on the vehicle

technology, type of fuel, maintenance and operating practices [2].

The awareness of this among the people, together with the effort of governments in creating laws to "punish" greenhouse emissions and favour low or zero emissions transportation is shifting the industry in investing in new vehicles and alternative fuels that are eco-friendly. In the case of HEV, the pollution is less because the gasoline engine works in its optimum point, while in the case of the EV tailpipe emissions are directly zero. This, of course, doesn't mean driving an EV is 100% clean because the vehicle must be manufactured and electricity has to be generated. If the energy comes, for example, from coal or heavy fossils, the emissions are even worse than in a conventional vehicle [4].

- **Prize of the energy:** In the case of pure EV, the price of the electricity is less than the one for petroleum. In the case of HEV, the combustion engine works at its maximum efficiency point, so for the same tank the distance that the vehicle can cover is higher, meaning the prize per km is lower. In the middle there are PHEV, which can work with cheap electricity or with the high efficiency of the HEV. In addition, places as public parking, universities or schools, working places or shopping malls offer free charging stations, so it can represent a huge saving compared with traditional vehicles, that overcomes the initial overrun that an electric vehicle means.

Having all these benefits, there are still some challenges that must be overcome in order to reach a more mature technology, as power electronics, electric machines, energy storage systems (batteries), better controls, thermal management... This master thesis is focused on the reduction and optimization of capacitors in the DC-link of power converters for a big hybrid electric vehicle, with the objective of having a lighter, smaller and cheaper capacitor in order to improve the reliability and cost of the overall system.

1.1 Objectives and thesis structure

As it was already mentioned, the main objective of this master thesis is to find ways of reducing the DC-link capacitor shared by the power converters in the vehicle. This reduction must be done in a such a way that the voltage levels are always among the limits impose by the normative, without compromising the good operating process of the system. In order to achieve it, the steps were the following:

1. **State of the art:** This is one of the most important steps in the thesis development. A large number of articles in different scientific journals (mainly the IEEE journal, since the university allows a free access to their members) were consulted and classified according to the methods used. If the article was not related to the topic it was discarded.

2. **Basic simulation files:** There was no previous work in this topic, so there was a need of creating a basic simulation which included the initial conditions of the vehicle before any modification. In this step, several parts of the simulation were created and tried independently. The main objective here was making sure that the initial capacitor selected by the company was enough to cover the DC-link variations.

3. **Final simulation and modifications:** When all the parts were working alone, they were merged together in a single file. After that, everything was prepared to try different options found during the documentation process.

1.2 System configuration

The power electronics system selected for the vehicle consists of two 3-phase inverters connected in a back-to-back configuration, fully bi-directional. The DC-link in the middle is connected to a DC/DC converter that transforms the high-voltage from the capacitor (600 V) into low voltage (28 V). This is shown in fig. 1-3.

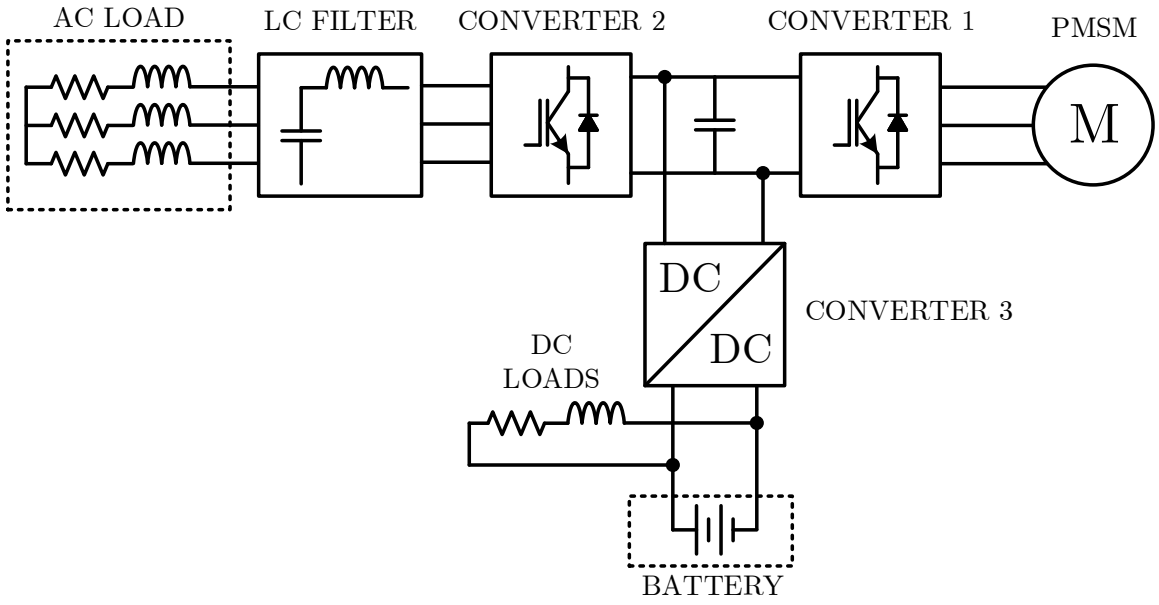

Figure 1-3: Power electronics configuration selected for the vehicle.

Both 3-phase converters are equal and made-up from 3 branches with 2 switches in each branch. One of the sides is connected to a 3-phase 75 kW electric motor, an Interior Permanent Magnet Synchronous Machine (IPMSM) coupled to a combustion engine. The other side has the option of being connected to an external 3-phase load by means of an LC filter, and needs to handle a maximum power of 70 kW. The load can be balanced or have a maximum allowed unbalance of 20%. Instead of a load, there can be an external power source injecting power to the low-voltage side. The third converter is a 17 kW DC/DC bidirectional converter, which can boost the voltage from the battery to levels of the DC-link, also allowing back the charge (from the electric motor acting as a generator or from an external source) in order to charge the batteries or feed low-voltage charges connected to that side. As a summary, there are three operating modes:

- **MODE 1. Export energy from the diesel engine:** In this mode, the vehicle is not running and the diesel engine is moving the electric motor, which generates electricity in order to maintain the DC-link with the **converter 1**, and feeds the external load connected to the 3-phase port. Batteries can be in three states: contributing with power, being charged or not working.

- **MODE 2. Motors not running:** In this mode, the vehicle is stopped as in the previous case, but this time the motors are not running. Batteries can be charged or discharged:

  - **Batteries charged:** There is an external power source charging the batteries and/or powering the low voltage loads. **Converter 2** maintains the DC-link voltage.
  - **Batteries discharged:** There are 3-phase loads connected to converter 2 being fed from the batteries, which are being discharged. Low voltage loads can also be fed. **Converter 3** (DC/DC) maintains the DC-link voltage. Loads connected in this case are limited by the power of the DC/DC, more restrictive than in MODE 1.

- **MODE 3. Vehicle moving:** During the normal operation of the vehicle, there can be load connected in the low voltage side of the DC/DC, which will be fed from the electric motor or the batteries, depending on the power requirements at each moment (the batteries can be charged or discharged). Converter 2 is disconnected for security reasons and **converter 1** maintains the voltage in the DC-link.

As a remark, the DC/DC converter with a battery was not in the initial designs and it was include later because it provides some improvements into the system, as an extra storage that can be crucial if there is a need of a power peak at a given moment. The other big benefit of having this converter is that it can balance the DC-bus voltage in a faster compared with the 3-phase converters, so this can lead to a capacitor reduction, which was properly checked during this thesis.

1.3 Capacitors in the DC-link

The DC-link capacitor in an electric vehicle is usually expensive, bulky and unreliable (due to its limited life cycle) and represents the most important passive component

of the system. It provides reactive power compensation, reduces power losses and maintains the voltage profile, decoupling the different converters in the system [5, 6]. When it comes the time to design the capacitor for an AC/DC/AC system, there are different parameters that influences the sizing. The most important ones are listed below [7]:

- Voltage ripple due to high-frequency components of the modulated DC currents of both converters.
- Inductor currents will flow into the capacitor if all the switches are open.
- Output power demand must be provided by the energy stored in the capacitor during the delay time associated with the voltage control loop, which can be speeded-up but never enough to avoid those peaks.

This last point is the most critical one in a classical system, determining the size of the capacitor. In our case the importance of this is less because there is an additional converter connected to a battery which may support the voltage and is able to react faster than the 3-phase converters. This can allow a further reduction of the capacitor size in comparison with the size when there is no DC/DC converter or battery.

The capacitor in the DC-link can be an electrolytic capacitor or a film one. Conventionally, they used to be electrolytic capacitors because the ratio between capacitance and volume (F/L) is much higher when compared to a film capacitor, meaning they can be smaller in size. However, its life-time is reduced (less than 10000 hours of use) and due to out-gassing phenomena, their capacitance is reduced along this time, being less safer. This doesn't happen to film capacitors, which have low ESR (equivalent series resistance) and ESL (equivalent series inductance) and high over-voltage capability [6]. Due to all of this, film capacitors are preferred, even when higher capacitances are more difficult to find commercially.

Independently of the technology, it is obvious that it would be really appealing to reduce the capacitor in the DC-link (reduce the value of the capacitance), for economic (initial price and maintenance) and reliability issues. Capacitor's lifetime

is mainly determined by the applied voltage and the core temperature. If one or both of these parameters increase, lifetime decreases. Since the voltage is fixed by the application, the only parameters that can be controlled is the core temperature. This temperature is determined by 3 parameters, the ambient temperature, thermal resistance and capacitor losses. Since the system of interest is a vehicle, the ambient temperature can't be controlled, and once the system is designed neither the thermal resistance, so the only parameter that is free to be controlled to increase the lifetime of the capacitor are the losses, being the most important one the thermal ones. These thermal losses are directly related to capacitor currents, so, as a conclusion, DC-link currents should be reduced in order to reduce losses and consequently increase the lifetime [6].

Chapter 2

State of the art

According to [6], methods to reduce the DC-link capacitor currents can be classified in three different categories, namely:

- **Modification of the inverter topology:** Current reduction due to a change in the classical power topologies.

- **Power balance control:** Consists of controlling the average current in the rectifier's side to make it equal to the inverter's side average current, balancing the instantaneous power imbalances so the only current flowing through the capacitor are unavoidable harmonics.

- **Modification of the PWM modulation scheme:** In general, these methods synchronize both converter's PWM signals or modified the classical modulation schemes. Improvements in the control systems' capacity in recent years have lead to an increased in popularity of this last method, forgetting more about the, sometimes, complex methods to balance the power.

In following sections there is a brief summary about these methods, specially regarding the last two since they are easier to implement on a system which is already known and/or built.

2.1 Power balance control

For this analysis, [7–10] have been considered. All of them deal with the subject of control schemes which improve the speed of controllers in order to reduce the stress in the capacitors during transients, consequently allowing a reduction in size.

Article [8] is relatively old, but highly cited by authors looking at the topic of capacitors reduction. Presenting a classic AC/DC/AC, it features a rectifier and an inverter, both controlled and fed from the grid and connected to an electric motor (induction motor because by the time the article was written PMSM were not so popular). In this case, the rectifier is in charge of keeping stable the DC-link voltage while the inverter controls the electric motor.

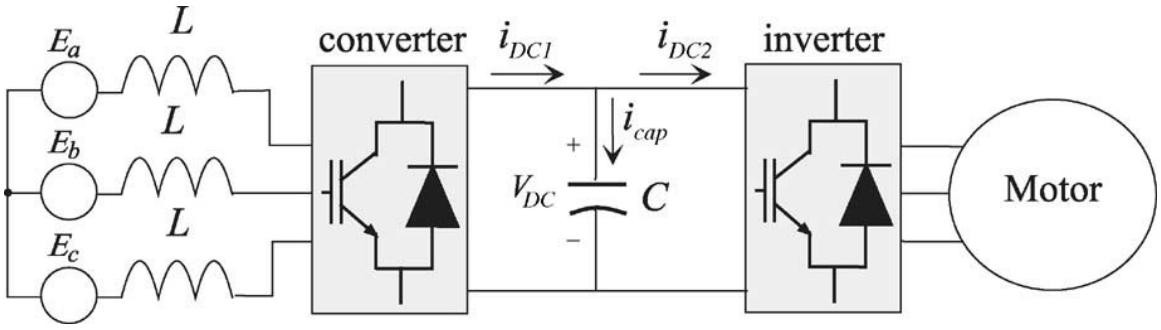

Figure 2-1: Configuration and power flow of the PWM converter–inverter system presented in [8].

The idea proposed in this paper consist of making equal both idc1 and idc2 currents, in such a way that there is no current flowing through the capacitor, thus no voltage variations. In order to achieve this current absence, the information of the current through the inverter is used to compensate in the rectifier's control loop as a feedforward term in the voltage node. With this, current through the capacitor is directly controlled and voltage variations in the capacitor are reduced for the same value of capacitor.

Due to these current control loops having an inherit delay (if PI gain is too high the loop is faster but there are issues with voltage limit and stability margin), it is not possible to make both currents exactly equal, so they also proposed a voltage compensation term, calculated based on a differentiator along with a predictive term

coming from the dynamics of both converters. This scheme with the differentiator can be seen in fig. 2-2, where it is compared with a classical scheme with load current feedforward compensation.

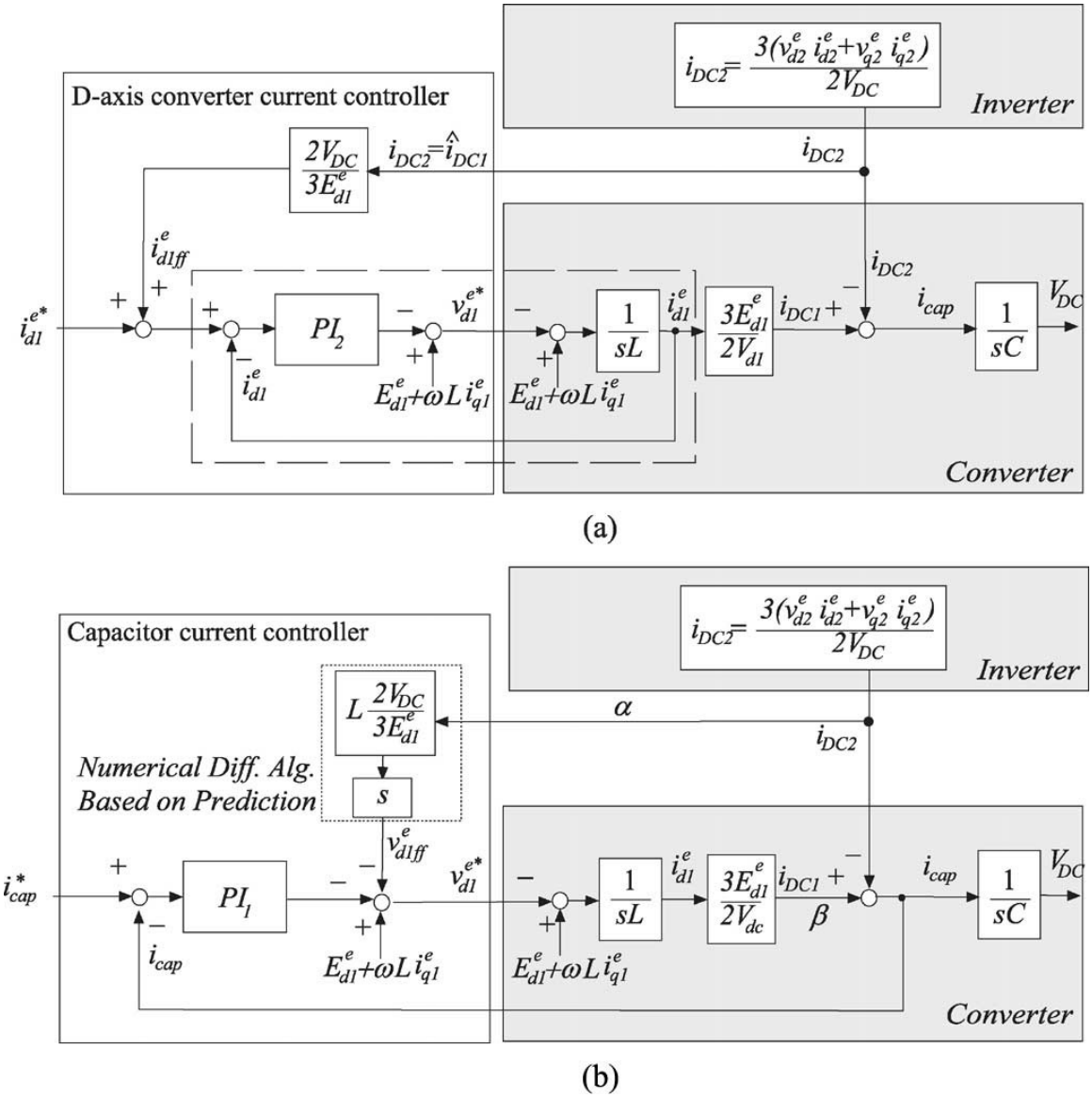

Figure 2-2: Conventional PI controller with load current feedforward compensation and proposed control improving the classical control thanks to a numerical differentiator [8].

The differentiator can cause several problems when it comes to adjust the control, so in [9] they propose a solution to avoid using it. The system is the same as in fig. 2-1 and it is assumed to have fast communication, so measures acquired in a given place

of the scheme can be used immediately anywhere. In order to avoid the use of a differentiator, current control loop for the motor includes an IP and not a PI. In the case of an IP controller, the gain does not lie in the forward path of the loop, so there is no need to differentiate currents id and iq. Motor current-control block diagram using IP controller is the one in fig. 2-3, where it can be appreciate the need for rapid communication between systems and the absence of differentiation.

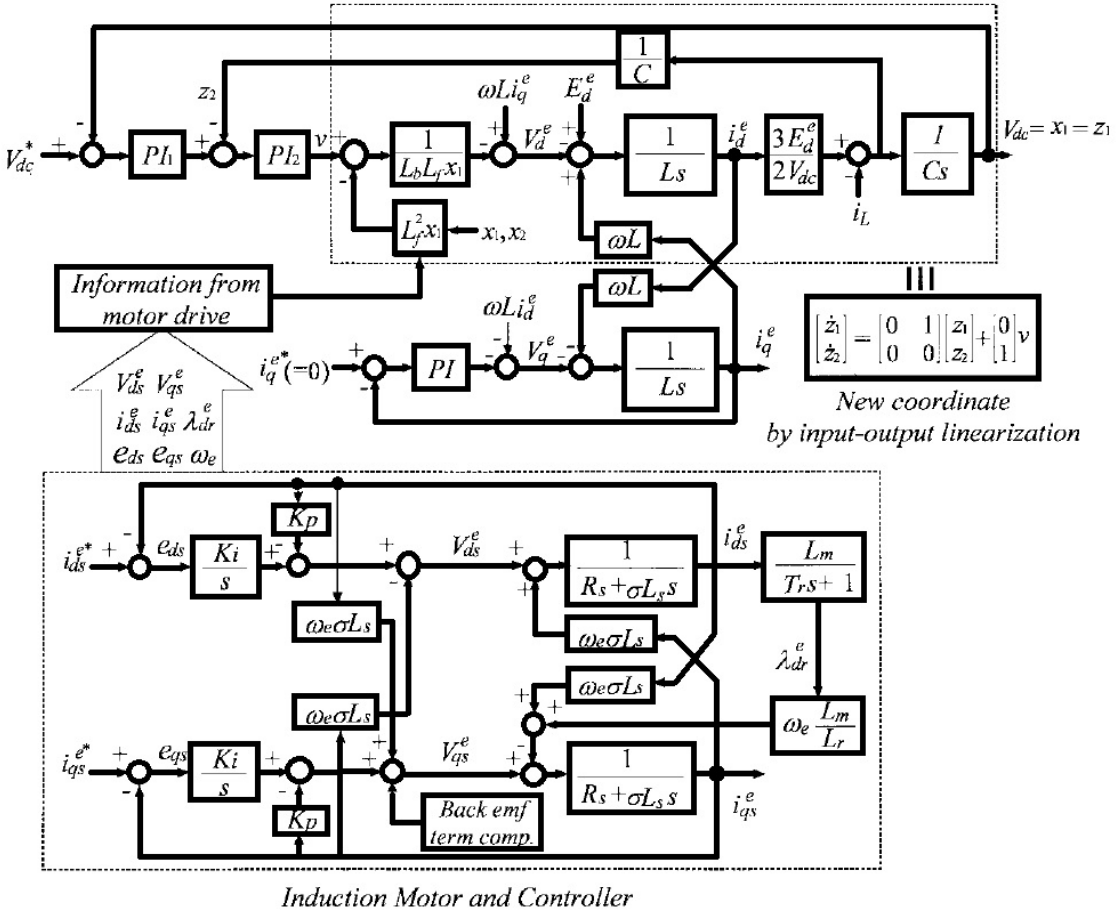

Figure 2-3: Nonlinear converter controller for the converter–inverter system presented in [9].

Other articles, as [7], emphasize also in the need of a fast control, using for example an hysteresis control. Even if it will never get to zero error, consequently producing variations in the DC-link, it is fast and easy to implement. They also recommend using feedforward current terms in order to improve the system response.

Finally, in [10] they present the idea of using active damping with the aim of stabilising the DC-bus. This method changes the dynamic impedance in the system by modifying the voltage output in the inverter introducing a virtual resistor, with the advantage of not generating losses as a real resistor would do. An additional current proportional to the voltage difference between the capacitor and the estimate voltage in the source (which is not measured in order to achieve load/source independent stabilization) will be injected (eq. 2.1) only if the system detects that the voltage in the capacitor is about to go out of the admissible range, so the dynamics of the controller won't be degraded when the system is working under normal conditions.

$$i_{damp} = \frac{V_{dc} - \hat{V}_s}{R_{damp}} \tag{2.1}$$

2.2 Modification of the PWM modulation scheme

References to this topic are in general more modern, as they take advantage of innovations in the fields of computers and electronics. Besides, different systems are studied, not only the classical AC/DC/AC (traditionally installed in industrial locations in order to control induction motors), but systems fed from batteries as a result of new portable applications as electric/hybrid vehicles. Articles [6, 11–17] have been analysed. In [11, 12] they present a DC/AC system with a bidirectional boost converter fed from batteries giving power to a 3-phase load (electric motor) by means of an inverter coupled to the boost with a capacitor, as seen in fig. 2-4.

They achieve a capacitor reduction by synchronizing the DC/DC converter with the inverter, making the switching frequency in the first one double the second, together with a carrier modification. An advantage of this system is the absence of complex control loops, since there are only modifications in the triangular carriers. In [12] they develop a related mathematical explanation about the same topic.

Following the synchronization topic, [6] presents calculations for obtaining the optimal phase shift angle between the two triangular carriers employed to control two converters in such a way that current harmonics through the capacitor are reduced.

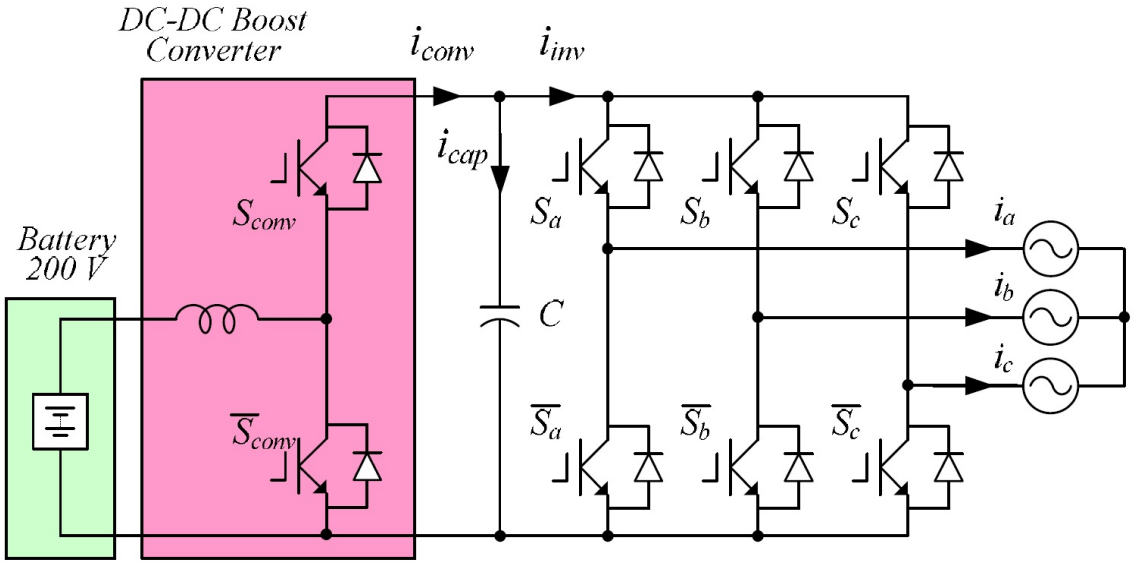

Figure 2-4: Schematic of a bidirectional DC-DC converter and an inverter feeding a 3-phase load as seen in [11].

The system is the one from fig. 2-5, having a motor/generator at both sides. The optimal interleaving angle (fig. 2-6) is related to the displacement power factor (DPF), modulation index and the modes of operation of both electric machines.

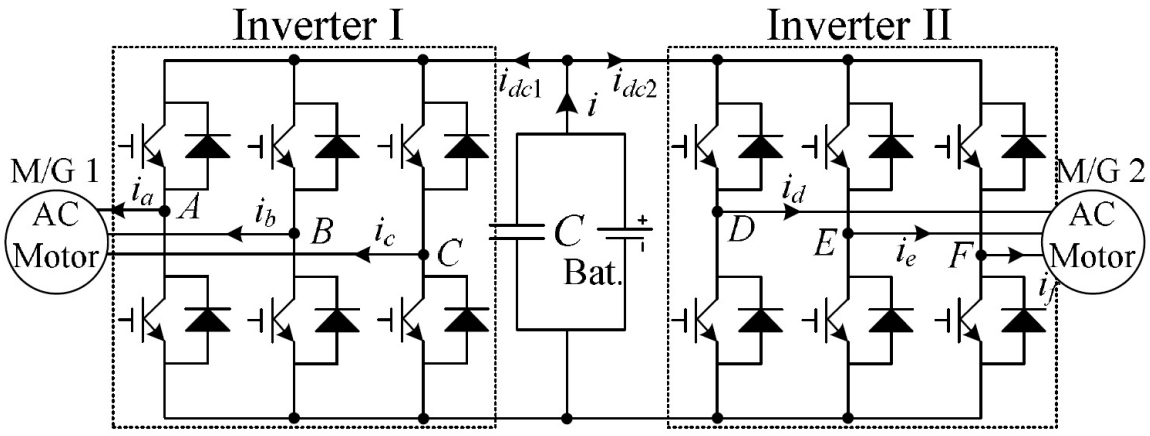

Figure 2-5: Power control unit architecture in [6].

This paper can be applied to the studied system considering that one of the motors in the scheme is the load connected to the vehicle (load can be connected both when the vehicle is stopped and moving). In this case, one side will always be occupied by an "electric machine" working as a motors demanding power to the other side,

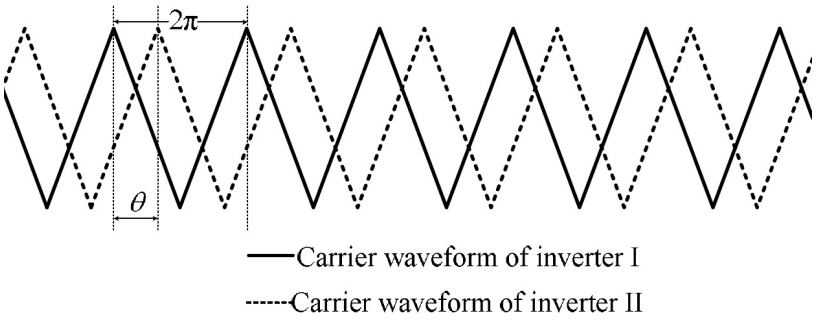

Figure 2-6: Definition of the interleaving angle for the synchronization of both converters [6].

therefore to the PMSM in the vehicle. This PMSM can work as a motor when the diesel engine is to be started or as a generator in normal operating conditions feeding the loads or charging the batteries. When the PMSM is working as a generator, the angle between both triangular waveforms should be zero (one "machine" motoring and the other generating from the diesel) for a minimum ripple, as reported by the article. In the case of having loads connected to the vehicle at the same time as the PMSM is acting as a motor to start the diesel the angle should be 90^o.

A different approach to the topic is presented in [13–16]. All these articles, from similar authors, are based on the analysis of the current in a switching period for the power topology in fig. 2-7. In this case, a three-phase load (electric motor) is fed from batteries by means of an inverter instead of being plugged in to the grid.

As it is already known, a classic inverter is formed by 3 branches with 2 switches in each one. The possible commutation states are 8, which are the ones that don't compromise the security of the system by either short-circuiting a branch or by creating an open-circuit that doesn't allow current control. 6 of these states are known as active vectors (V1-V6) and the other 2 as zero vectors (V0 and V7). This is shown in fig. 2-8.

Space vector PWM (SVPWM) generates the desired vector by means of two adjacent active vectors and uses one or the two zero vector to complete until the end of the period. By using these two adjacent vectors, the total harmonic distortion (THD) is minimized. When the zero vectors are applied, current becomes zero, as seen in

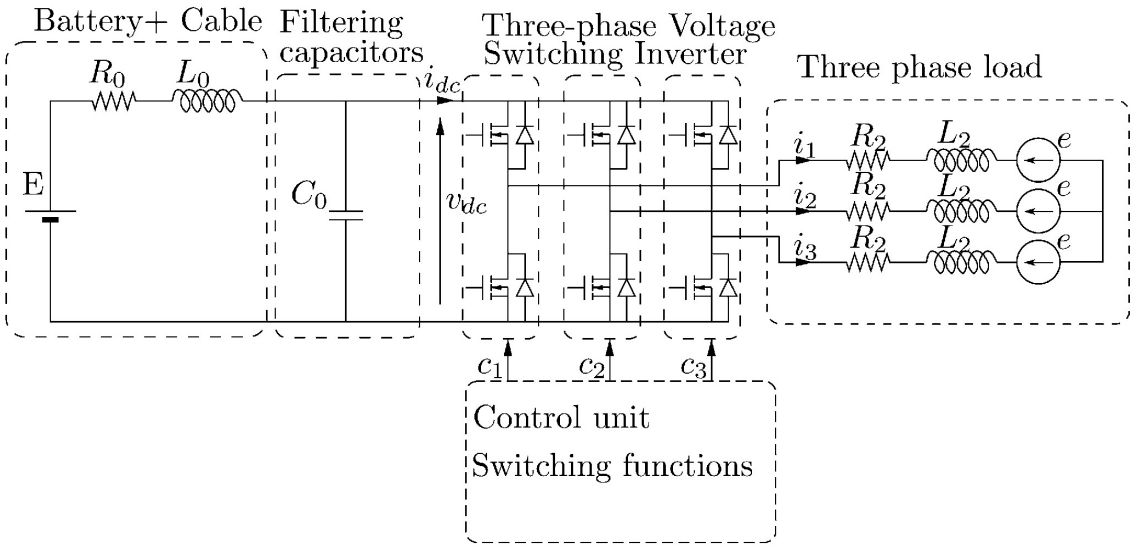

Figure 2-7: Architecture of an embedded electric power train system according to [16].

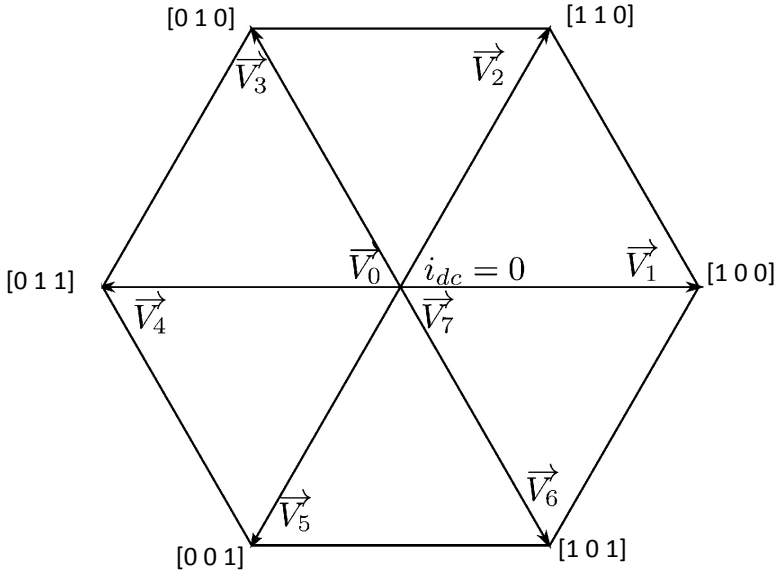

Figure 2-8: Distribution of the 8 possible control vectors in a d-q plane when using vector control [16].

fig. 2-9. These 2 vectors are responsible of the difference between the mean value and the instantaneous value of the current through the capacitor, causing fluctuations in the voltage.

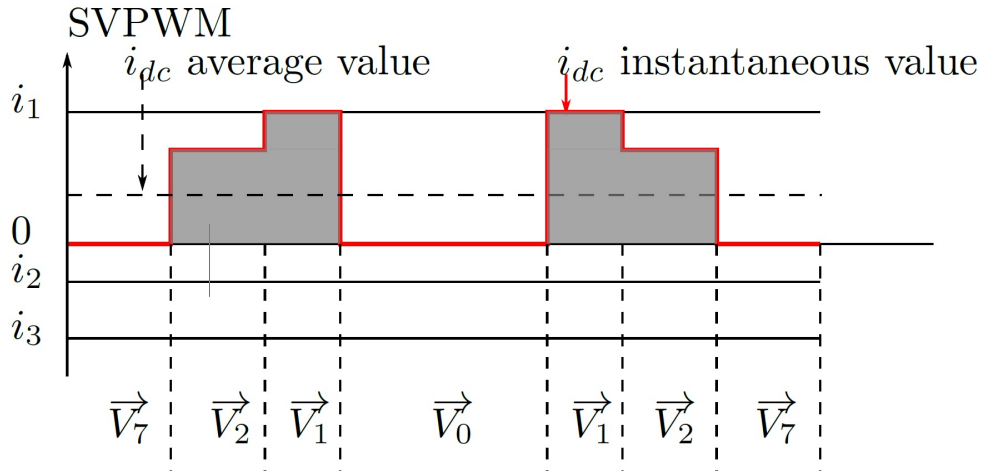

Figure 2-9: Average and instantaneous value of idc over a switching period with SVPWM when the modulation index is below 2/3 [15]. The distribution of the vectors like this causes a minimization of the THD.

To avoid or reduce the fluctuation, authors of these papers suggest using non-adjacent vectors or more than 2 active vector in order to obtain the same initial vector but with a reduced or removed zero time, depending on the modulation index. These vectors must never be opposite vectors, since it will cause an inversion in the instantaneous value of the current through the capacitor in the switching period. Depending on the modulation index, vectors should be 3 if the indexes are high ($\geq$2/3) or 2 non-adjacent and a zero vector in the other case. In this last option, the zero time will be always lower than in the classical SVPWM. Along the 4 different articles, authors improve the proposed method, which is finally called Extended Double Carrier PWM Strategy [16]. It can be used for a varied range of modulation indexes and loads with high power factor ($cos\varphi \geq 0.8$). A drawback of the method is that the load current quality is reduced (higher THD), even if with high modulation indexes it can still be compared.

In between control loops or modulation modifications there are some papers as the one in [17], where they want to substitute an electrolytic capacitor by a ceramic

one in an AC/DC/AC system, as the one in fig. 2-1. The system consists of an AC-DC active front-end (AFE) converter, a DC-AC voltage source inverter (VSI), and a 10 μF ceramic capacitor in DC link. In order to achieve this capacitor reduction, a PWM modification (that reduces common mode voltages) is applied together with some control techniques, such as a feedforward term from the current in the PMSM, as it was explained in subsection 2.1. Control block for this case is presented in fig. 2-10, which includes this feedforward term.

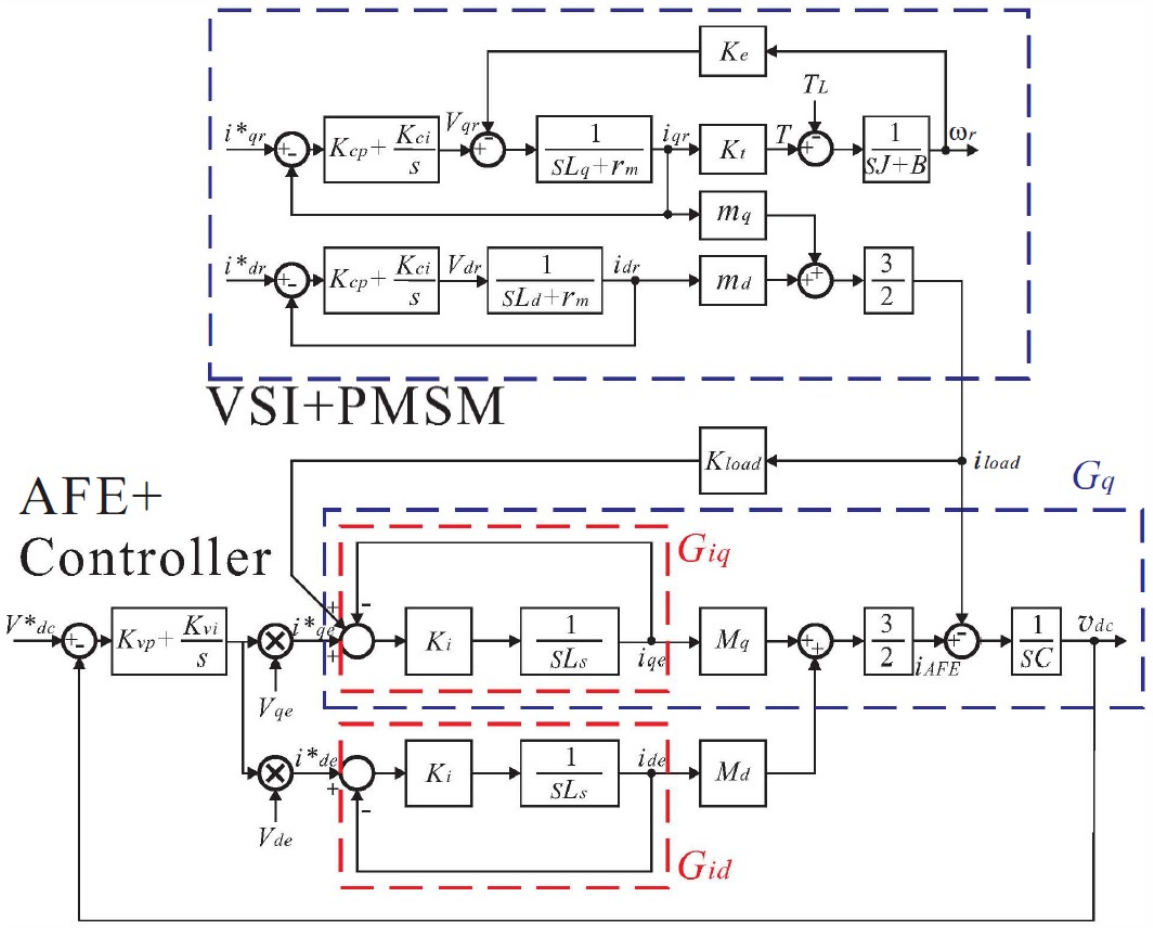

Figure 2-10: Control block diagram of the AC-DC-AC converter system in [17].

This article propose a modified SVPWM in order to use non-adjacent and opposite vectors, even when previous authors advised against it.

2.3 Modification of the inverter topology

These systems modify the basic structure in a power system in order to take advantage of an interesting characteristic, as adding additional switches, change their position or use interleaving techniques in order to reduce current or voltage ripple. This topic was not deeply studied since the topology is already defined. Nevertheless, some examples are briefly presented, [18, 19]. In [18] a DC/AC system is used to control a motor, but the classic boost converter is substitute by a modification with coupling inductors. This way, they claim to achieve overall cost reduction and switching loss improvement, reduction of the PWM ripple content on the AC motor and smaller filter capacitor. As a drawback, the system is not a typical one so it is less known, and the need of coupling power inductors adds complexity to the system and the control. In addition, control speed must be increased.

Finally, [19] presents a power topology joining several boost converters in an interleaving scheme sharing the DC-link, achieving some harmonic cancellation. This article searches for the optimal switching pattern for the boost converters' phases and the DC-link voltage level starting from a general analytical expression for the DC-link capacitor RMS current and depending on the operational point.

2.4 Conclusions

It can be concluded that for using control techniques in order to reduce the capacitor in the DC-link based on power balance control is necessary to have good communication between all the parts forming the converters system, in order to have the information available anywhere and be able to realize the appropriate couplings. Methods such as feedforward in order to anticipate for the current demand and react in a faster way avoid strong variations in the capacitor's current, which results in a voltage variation, allowing for a capacitance reduction in the same system. "Virtual" modifications in the system, as active damping, could also help when it comes to stabilize the DC-bus voltage under heavy power changes.

In the other hand, modification of the PWM modulation can be done by changing the triangular carrier or by changing the selection of the vector when applying SVPWM. The fact of trying to synchronize the converters in the system in such a way that current fluctuations are reduced seems a tendency.

Finally, some benefits may be extracted from a modification in the power topology, but that would mean changing the design and using topologies not so well-known or studied, so they should only be selected when the benefits are clearly higher than the cost of studying and implementing a different topology.

Chapter 3

Simulations

This chapter presents the simulations carried out during the development of this master thesis. In order to validate techniques for capacitor reduction, the first step was to build a simulation model of the system as detailed as possible. Different parts of the system were modelled separately and then joint together in a bigger simulation using the starting value of the capacitor. The different parts that were simulated individually are:

1. Electric motor with fixed speed input.

2. Simplified diesel model.

3. External load fed from ideal voltage sources.

Once they were working, the first and second simulation were merged together, after that the effect of a simplified DC/DC was added and finally the third simulation was also built-in in order to get to the final one. After that, everything was ready to try different things in order to see the effect in the stability of the DC-link. As it was mentioned in chapter 1, there are 3 different modes of operation. Among them, it is considered that the one affecting more the DC-link is MODE 1, because load changes here can be more abrupt (MODE 2 is limited by the power of the DC/DC, which is less, so load changes are smaller).

3.1 Electric machine

The electric machine used in this project is an IPMSM, as selected by the company. The most important reasons to use interior (buried) magnets and not surface mounted here are:

- Magnets are more protected, since if the speed increases with SPMSM the magnets could get detached.
- IPMSM achieve higher torques due to the asymmetries in the construction.

As drawbacks, they are more difficult to build because the magnets must be inserted in the interior of the stator and they are also more difficult to control, precisely because of those asymmetries.

3.1.1 Mathematical model of an IPMSM

The stator phase voltage equation for a PMSM is shown in eq. 3.1 [20].

$$\overrightarrow{V^s_{abc}} = R_s \overrightarrow{I^s_{abc}} + \frac{d}{dt}\overrightarrow{\lambda^s_{abc}} \tag{3.1}$$

Where:

- $\boldsymbol{R_s}$ **(Ω)** $\longrightarrow$ Stator phase resistance.
- $\boldsymbol{\overrightarrow{I^s_{abc}}}$ **(A)** $\longrightarrow$ Stator phase current.
- $\boldsymbol{\overrightarrow{\lambda^s_{abc}}}$ **(Wb-t)** $\longrightarrow$ Flux linkage measured in Weber-turns.

This equation is transform to a dq reference frame and divided in d and q axis. In appendix A there is a brief summary on this reference frame. D-axis stator voltage equation is presented in 3.2 and q-axis stator voltage equation in 3.3.

$$v^s_d = R_s i^s_d + \frac{d}{dt}\lambda^s_d - \omega_e \lambda^s_q \tag{3.2}$$

$$v_q^s = R_s i_q^s + \frac{d}{dt}\lambda_q^s + \omega_e \lambda_d^s \tag{3.3}$$

Where:

- $\boldsymbol{i_d^s}$ **and** $\boldsymbol{i_q^s}$ **(A)** $\longrightarrow$ Stator currents in dq reference frame.
- $\boldsymbol{\lambda_d^s}$ **and** $\boldsymbol{\lambda_q^s}$ **(Wb-t)** $\longrightarrow$ Stator flux linkages in dq reference frame.
- $\boldsymbol{\omega_e}$ **(rad/s)** $\longrightarrow$ Electrical speed.

Last term in both equations is normally referred to as *cross coupling terms*, because they coupled both axes. They are an effect of the transformation. When controlling a PMSM, the d-axis is usually aligned with the PM flux rotating vector, in such a way that the magnet flux reflected in the q-axis becomes zero [21]. Axes orientation is shown in fig. 3-1.

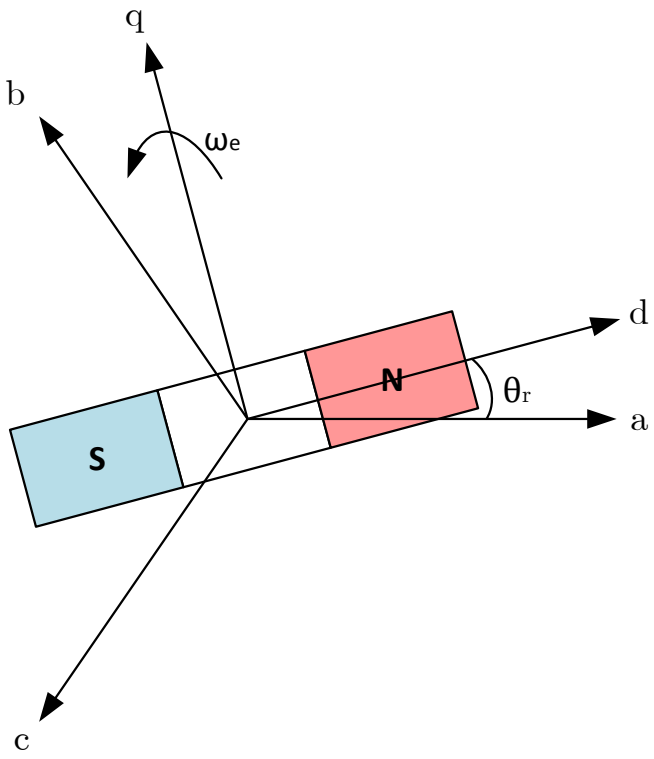

Figure 3-1: Abc to dq axes transformation in a 2 poles PMSM.

Proceeding like this, the flux linkage in both axes can be written as eq. 3.4 and eq. 3.5.

$$\lambda_d = L_d i_d^s + \lambda_{PM} \tag{3.4}$$

$$\lambda_q = L_q i_q^s \tag{3.5}$$

Where:

- $\boldsymbol{L_d}$ **and** $\boldsymbol{L_q}$ **(H)** $\longrightarrow$ d and q stator inductances.
- $\boldsymbol{\lambda_{PM}}$ $\longrightarrow$ Permanent magnet flux.

Finally, using previous equations, stator voltages in dq reference frame can be expressed as eq. 3.6 and eq. 3.7.

$$v_d^s = R_s i_d^s + \frac{d}{dt}\lambda_d^s - \omega_e L_q i_q^s \tag{3.6}$$

$$v_q^s = R_s i_q^s + \frac{d}{dt}\lambda_q^s + \omega_e L_d i_d + \omega_e \lambda_{PM} \tag{3.7}$$

3.1.2 PMSM model in Simulink

For the simulation of the motor, the model of a Permanent Magnet Synchronous Machine (PMSM) was selected in Matlab Simulink, with salient-pole rotor type. The real model is an electric machine designed specifically for this application by the company, and its data is provided in table. 3.1.

From these information, some of the required parameters had to be computed in order to complete the model, particularly the stator phase resistance and the flux. They provided cooper losses and phase current at nominal speed, so the resistor is calculated as in eq. 3.8.

$$R_s = \frac{P/3}{I^2} \tag{3.8}$$

Variable	Units	Value
Pole Pairs (P)	-	6
Nominal Speed (N)	rpm	6500
Phase to neutral voltage (Vrms)	V	150
Phase current (Irms)	A	171
Power (P)	kW	75
Cooper losses	W	1580
Ld	mH	0.096
Lq	mH	0.209

Table 3.1: IPMSM data as provided by the company. Currents, voltages and power are given at nominal speed.

Where:

- $\boldsymbol{R_s}$ **(Ω)** $\longrightarrow$ Stator phase resistance.
- **P (W)** $\longrightarrow$ Power losses in the cooper. They have to be divided between the number of phases because the nominal current is given per phase.
- **I (A)** $\longrightarrow$ Current in rms value per phase at nominal power.

For the magnetic flux calculation, the equation applied is the one in 3.9 [22]. Note that $\omega_r P$ represents the electrical speed.

$$\lambda_{PM} = \frac{BEMF}{\omega_r \cdot P} \tag{3.9}$$

Where:

- **BEMF (V)** $\longrightarrow$ Back Electromotive Force expressed in phase to neutral peak.
- $\boldsymbol{\omega_r(rad/s)}$ $\longrightarrow$ Mechanical speed from the rotor of the electrical machine.
- **P** $\longrightarrow$ Pole pairs to transform mechanical speed into electrical speed.

Finally, in order to make the simulation as real as possible, the model includes values for inertia and viscous damping. The inertia includes not only the one for the electric motor but for the whole system (load), so it was selected big enough to

represent a big vehicle, in such a way that a load change didn't almost affect the speed.

3.2 DC-link voltage control

In the mode of operation selected, the converter connected to the IPMSM is the one maintaining the voltage in the DC-link. In order to do so, two nested loops are prepared, one inner and faster loop for the current and a slower one for the voltage, with enough difference in bandwidth so the interferences between them can be neglected. The control is realized in a dq synchronous reference frame.

3.2.1 Current control loop

The current is controlled to be aligned with the q-axis, which means aligned with the BEMF (BEMF is proportional to the magnetic flux, as it was seen in eq. 3.9). This decouples torque and flux in the machine. It is important to note here that d-axis current must be forced to zero by the controller, since it does not naturally stays at zero. When the PMSM is acting as a motor, negative direct current is sometimes used when working at high speeds, because that "weakens" the flux, reducing the BEMF and allowing to work at higher speeds because there is more voltage available [21, 23]. Since in this case the machine acts as a generator there is no interest in reducing the BEMF.

Both d and q current loops are shown in fig. 3-2. Quantities with an asterisk represent references, the rest of them are known values or measured ones.

The error in the current is introduced to a PI, which is tuned as explained below, in subsection 3.2.1.1, with a bandwidth of 500 Hz. The voltage coming out of the PI is transformed by means of the cross coupling terms that appeared due to the axes transformation shown in equations 3.6 and 3.7. Q-axis includes also the compensation of the BEMF that only appears there due to the alignment during the synchronization.

In order to obtain the current measurements needed for the loop, stator currents in abc are measured and transformed to dq. As it was already mentioned, the basics of

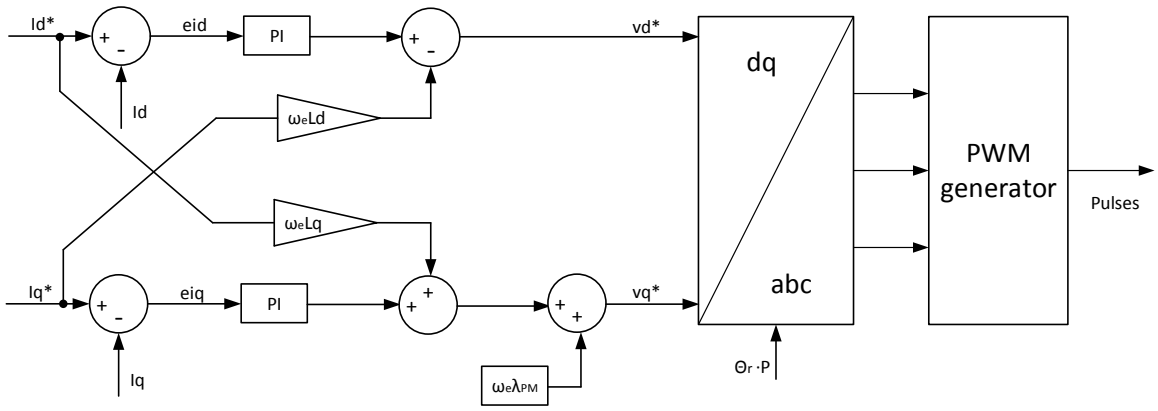

Figure 3-2: Current control loop for the generator with pulse generation.

this transformation is the synchronization of the axes in such a way that the complex vector rotates at the same speed as them, so there is a need of a synchronization angle. This angle is obtained from the position of the rotor (tracking the position of the magnets), this way having everything rotating at the same speed. Obviously, the position of the rotor must be measured precisely, otherwise there will be an error and the loops won't be working properly. This measurement can be done by means of a sensor mounted on the shaft based on different technologies, or estimated in a sensorless way. For all the simulations it is assumed that the position is well known at every instant because position measurement is not the objective of this thesis.

Once the voltage in dq synchronous reference frame are obtained, they are transformed to abc using the inverse transformation and the same angle, and with those quantities it is now possible to generate the pulses for the rectifier (converter 1 in fig. 1-3). Pulse generation from abc references using comparisons with triangular carriers is summarize in appendix B.

A demonstration of these current loops working is shown in fig. 3-3. For this simulation, the generator is running at a constant speed of 4500 rpm and fed from a constant 600 V DC voltage source, with the converter switching at 10 kHz. Id reference is set to zero and iq is varied from -30 A to -60 A at 0.25 s. As it can be seen, both currents track the reference correctly with a ripple that is due to the switching effects in the converter.

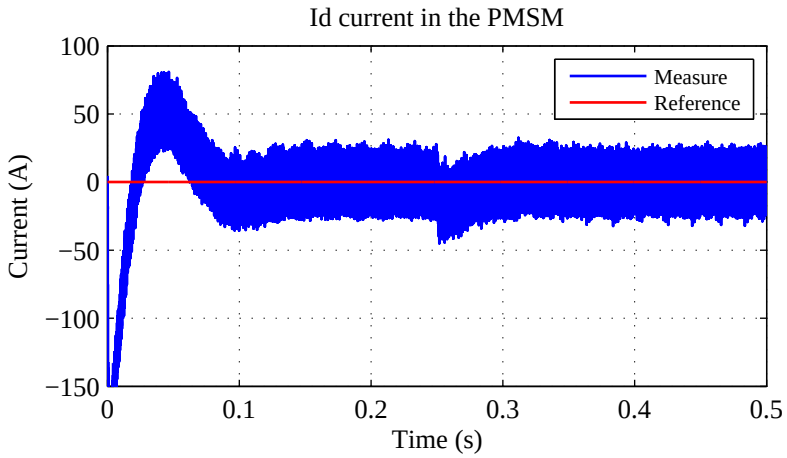

(a) Id

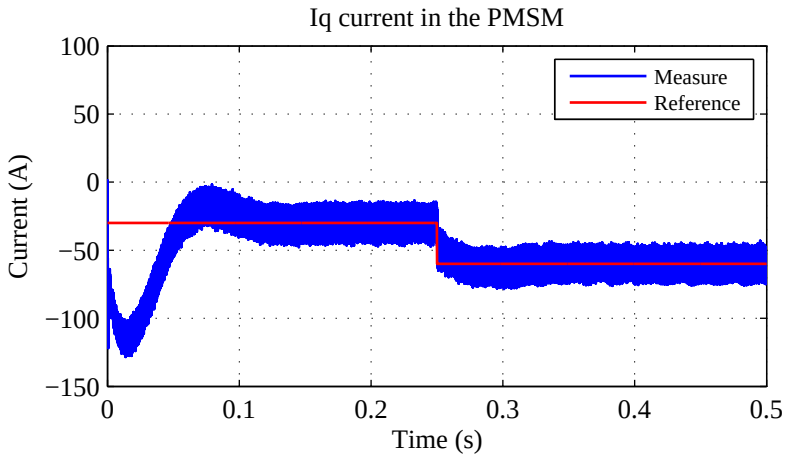

(b) Iq

Figure 3-3: Current in id (3-3a) and iq (3-3b) axes from the generator when the capacitor is substitute by a constant voltage source and there are only current loops in the control.

3.2.1.1 PI controller for the current loop

A general PI controller has the form of eq. 3.10, with K being a proportional gain and c the zero.

$$PI(s) = \frac{K(s+c)}{s} = \frac{Ks + Kc}{s} \tag{3.10}$$

The plant for the current loop, G(s), is the one from eq. 3.11. It is a simplified model of an electric motor considering it as an RL load, being R the stator phase resistance and L the inductance (first order system). When working in d and q

coordinates having asymmetries in the rotor (IPMSM), L will be L_d or L_q depending on the axis to be tuned.

$$G(s) = \frac{1}{Ls + R} = \frac{\frac{1}{L}}{s + \frac{R}{L}} \tag{3.11}$$

The scheme with the position of the PI and the plant is shown in fig. 3-4.

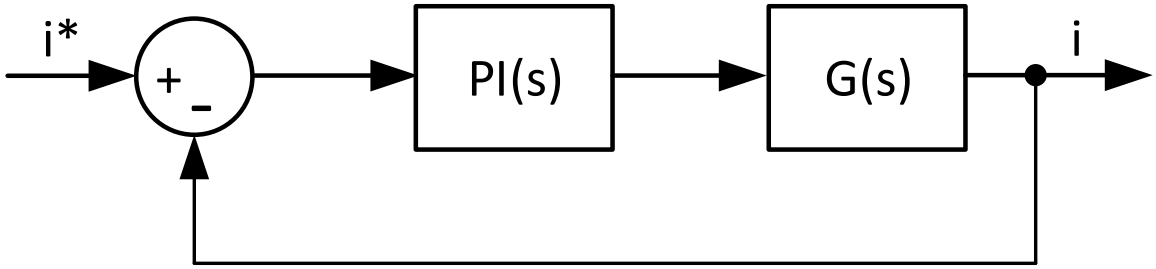

Figure 3-4: General scheme for the current loop with a PI regulator.

Because of the controller and the plant being in series, the combined block can be expressed as eq. 3.12.

$$G_T(s) = PI(s) * G(s) = \frac{K(s + c)}{s} \frac{\frac{1}{L}}{s + \frac{R}{L}} \tag{3.12}$$

The most interesting thing for this control is to cancel the pole of the plant with the zero of the controller. This can be done if the value of the zero is R/L. After the zero-pole cancellation has been made, the transfer function is reduced to $\frac{K}{sL}$. The final expression for the block is then the one in eq. 3.13, with $\frac{K}{L}$ being the bandwidth (ω) of the system.

$$G_T(s) = PI(s) * G(s) = \frac{\frac{K}{L}}{s + \frac{K}{L}} \tag{3.13}$$

Bandwidth ω of a system can be expressed as 2πf, so the final expression for K is shown in fig. 3.14.

$$K = 2\pi f L \tag{3.14}$$

In Simulink, the transfer function of a PI controller can be expressed in two analogue ways, parallel or ideal. Parallel connection is shown in eq. 3.15, with P being the proportional constant and I the integral action.

$$PI(s) = P + \frac{I}{s} = \frac{Ps + I}{s} \tag{3.15}$$

Since the first expression for a PI shown in eq. 3.10 and this last one are the same, the final values in Simulink for the proportional and integral actions are:

$$\mathbf{P = K}$$
$$\mathbf{I = K \cdot c}$$

3.2.2 Voltage control loop

Voltage control loop generates the current command for the q-axis in order to maintain a desired voltage in the DC-link. In this case, it is a fixed value of 600 V. In the d-axis there is no voltage control because the current is already being controlled to zero for the axis alignment. The basic control scheme is shown in fig. 3-5.

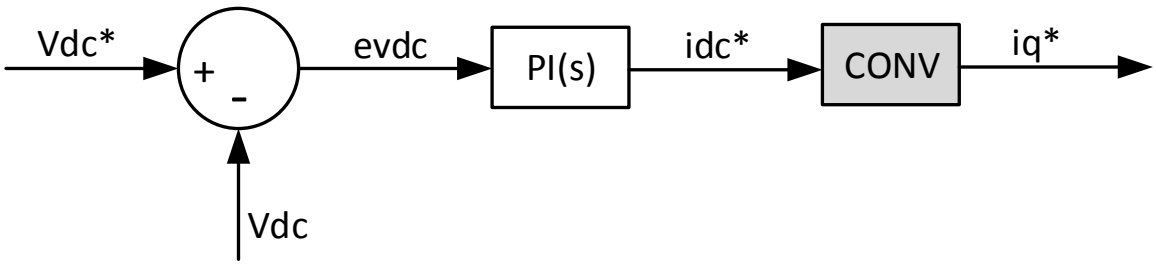

Figure 3-5: Voltage control loop for the generator.

The error in the voltage is introduced to a PI, with an smaller bandwidth compared to the current loop (60 Hz), and its output is the DC current needed to maintain the voltage in the DC-link. Since we have to work with currents in dq reference frame in the AC side of the converter, there must be a transformation between both sides. This is done assuming there are no losses in the converter so the power is conservative.

The assumption is valid because power electronics converters in general have high values of efficiency. This is shown in eq. 3.16. BEMF voltage needs to be expressed in peak to peak rms, and it can be computed using eq. 3.9.

$$P_{DC} = P_{dq} = V_{DC} I^*_{DC} = \sqrt{3} \cdot \frac{BEMF}{\sqrt{2}} \cdot \frac{iq^*}{\sqrt{2}} \tag{3.16}$$

The final equation to perform the transformation is shown in eq. 3.17.

$$iq^* = \frac{2V_{DC} \cdot I^*_{DC}}{\sqrt{3} BEMF} \tag{3.17}$$

For the tuning of the voltage PI, the current loop is assumed to be so quick that it can considered instantaneous. This way, the plant G(s) is only the capacitor. Using sisotool (another Matlab tool) with that plan, the values for the proportional and integral action were obtained.

3.2.2.1 Voltage limits: normative

The company provides the limits for the voltage in the DC-link that it is mandatory to follow when working at any mode and any condition. Fig. 3-6 shows the maximum and minimum voltage allowed during normal operation ($\pm$35 V) and during transients. The ripple amplitude allowed are 9 V with a distortion factor of 0.015.

3.3 Diesel engine modelling

The model of the IPMSM can be fed from torque or speed. Initially, the simulation was fed from a fixed value of speed. In order to make it more realistic, the input was changed to torque to include the effects and limitations of the diesel engine. This is done by considering a simplified model of the real engine using data provided by the manufacturer. The model is the Detroit DD15 Engine from the manufacturer Detroit. The maximum power, 339.29 kW, is obtained at 1625 rpm and the maximum torque, 2102 Nm, at 975 rpm [24]. The datasheet includes horsepower and torque curves. The data from these curves were extracted manually in order to have a representation of

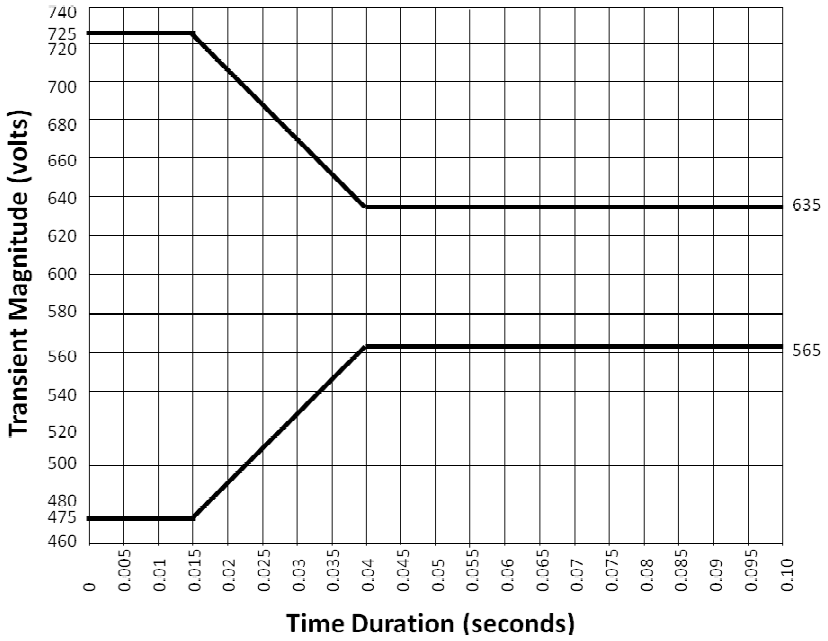

Figure 3-6: Voltage limits in the DC bus, including transients.

the complete curves in Matlab with the idea of using them in the simulation. They are shown in fig. 3-7.

A speed control was implemented in order to generate the torque representing the coupling between the diesel engine and the electric generator. The error in the speed of the rotor is introduced to a PI tuned in such a way that the output is the torque required to maintain the reference speed, with a bandwidth of 100 Hz. Proportional gain and zero of the controller are computed by zero pole cancellation as in section 3.2.1.1, using values of inertia and damping instead of inductance and resistance (in that order).

Since the electric generator is moving thanks to being coupled to the diesel engine, this last one is the one who provides the torque requirements, and the maximum value that it can provide changes according to the speed. Using the torque-speed curve from fig. 3-7b it is easy to know the maximum at each speed, so the effect of the diesel appears in the simulation as a variable saturator limiting the requirements of the speed PI. A diesel generator can't provide negative torque, so the saturator always limits to zero as the lower bound. It is interesting to mention here that there is a

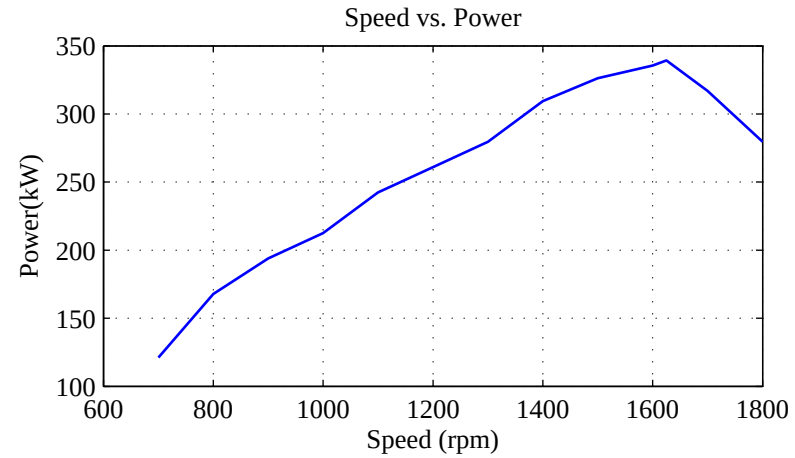

(a) Power

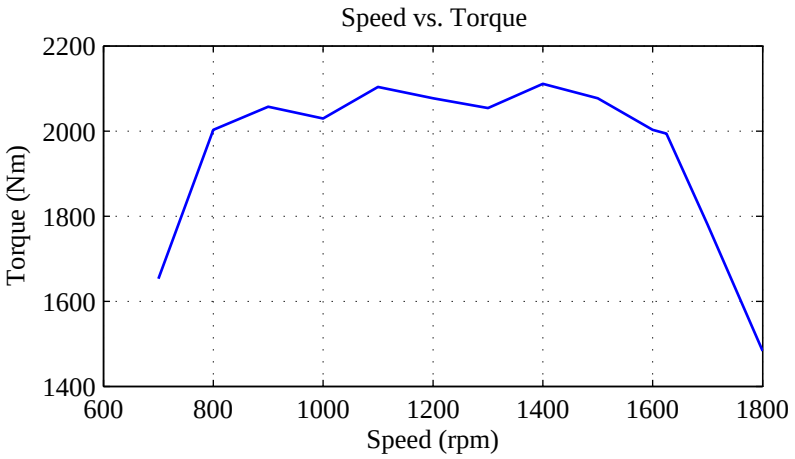

(b) Torque

Figure 3-7: Power (3-7a) and torque (3-7b) curves for the DD15 engine.

gearbox between both machines, they are not coupled directly. For the simulations it is considered a fixed ratio of 1800/6500, which are the nominal speeds for the diesel engine and the PMSM respectively. This is all shown in fig. 3-8.

As a final comment, there is no torque production in the diesel engine if the speed is under 700 rpm. For this simulations we consider that the engine has been previously started by other means, as using the PMSM as a motor instead of a generator. If the speed goes below the minimum during the simulation, the maximum torque available from the diesel engine is fixed to the one that can be produced at 700 rpm.

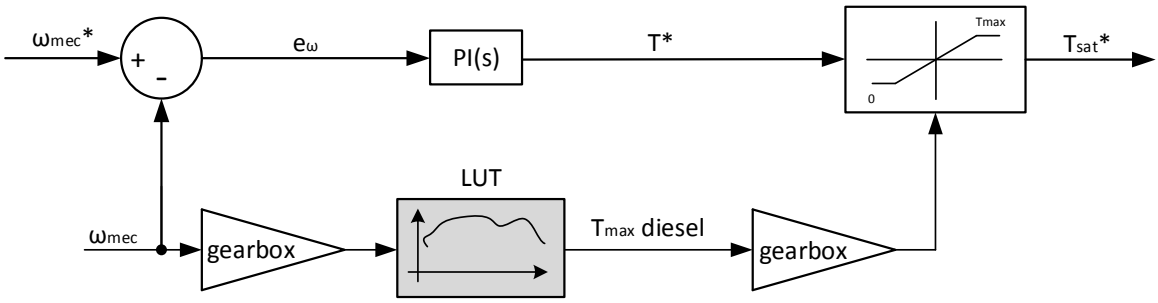

Figure 3-8: Speed control loop using the diesel engine torque-speed curve as a limitation at different speeds.

3.3.1 Simplified simulation with the diesel engine

In order to demonstrate the proper functioning of this simplified model of a diesel engine coupled to a PMSM, control from fig. 3-8 is implemented in Simulink connected to a first order transfer function (eq. 3.18) of the mechanical model of a vehicle defined by its inertia and damping instead of the real model of the machine, in order to avoid high simulation times.

$$G(s) = \frac{1}{Js + b} \tag{3.18}$$

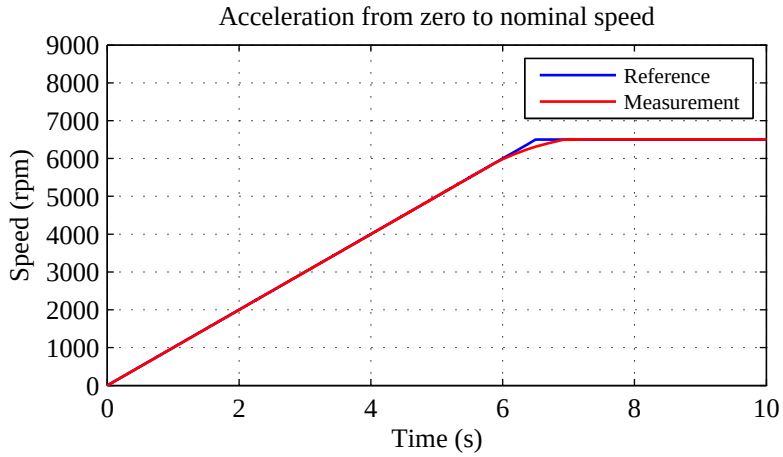

Figure 3-9: Speed command for the PMSM and the real speed following the reference when the electrical machine is simulated as a first order transfer function.

The speed command is varied from zero to nominal speed in 6.5 seconds and

then stays at that speed. The variation must be done smoothly because the inertia constant is high and it is not realistic to vary the speed in steps. The speed following the reference ramp is shown in fig. 3-10. Even if it is not seen in the figure because it is very small, it is interesting to remark that the tracking during the ramp is not done without error because the PI makes the error zero only in steady state. Anyway, this error is negligible.

Maximum torque used for the saturator is shown in fig. 3-10. At the beginning, and before the speed in the diesel reaches 700 rpm, the torque available is forced to the minimum at that speed as explained before. After that, it can be seen how the graph changes with the same shape as in fig. 3-7b. After reaching nominal speed, (1800 rpm for the diesel), the maximum torque available is constant and has the same value as the last point in the forementioned speed vs. torque curve for the engine.

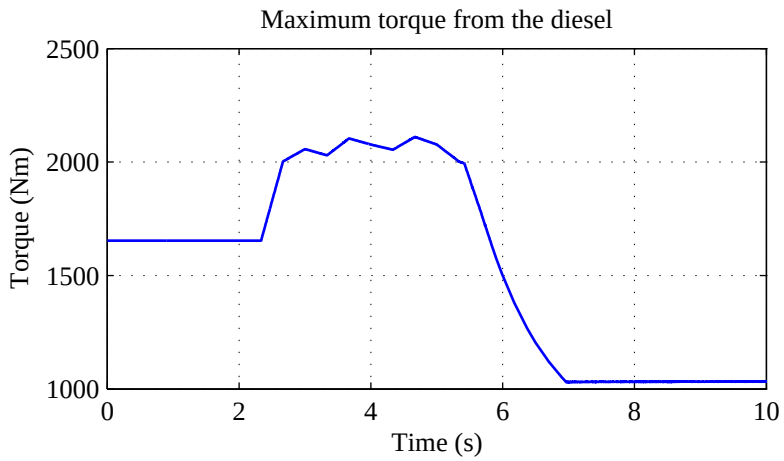

Figure 3-10: Maximum torque that the diesel engine can provide at every moment depending on the speed. It does not mean that it is providing this torque, just shows the capability.

3.4 PMSM and diesel model integration

One of the most difficult tasks in this thesis was simulating the electric motor generating power in order to maintain the DC-link voltage constant while coupled to the simplified model of the diesel. Once previously explained models for the control

of the power extracted from the generator and the model of the diesel engine were working, they were merged together and checked.

In this model, the rectifier connected to the PMSM is controlling the voltage in the capacitor and feeding some DC resistive loads (single-phase). In order to test this new model, the speed was kept constant at 4500 rpm and the simulation started with some speed in the PMSM as initial condition, in order to get sooner to the reference and being able to simulate everything in a short period of time (more simulation time means more real time spent in the simulation and lack of memory space in the computer in order to save the resulting data). The power demanded by the loads were changed during the simulation: initially, there are no loads so the power demand is zero. At 0.3 seconds there is a step in the demand of 24 kW and at 0.6 seconds this demand disappears again. The simulation ends at 0.8 s. Resulting DC-link voltage is shown in fig. 3-11. This image includes the reference and the real value alongside voltage limits in steady state as explained in subsection 3.2.2.1. As it can be seen, whenever there is a power change in the demand the capacitor gets charged or discharged, which is reflected in the voltage. In the case presented, there are no problems of violations of the normative. Anyway, this is not the most adverse case because the objective of this graph is to show the control of the DC-link voltage working.

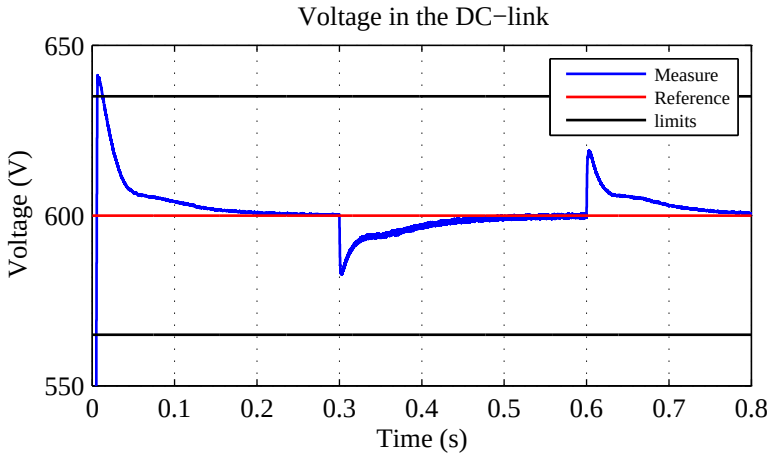

Figure 3-11: Voltage in the DC-link when the generator is feeding resistive DC loads.

3.5 DC/DC converter

The DC/DC converter between the battery and the DC-link was not fully defined by the company at the moment of realization of this thesis. What is known is that it is a 17 kW converter, transforming from 26.4 V in the battery to the 600 V in the DC-link.

3.5.1 Battery

The battery placed at the low voltage side is rechargeable and manufactured in lithium-ion. The most important data is shown in table 3.2.

Variable	**Units**	**Value**
Nominal capacity	Ah	60
Nominal voltage	V	26.4
Voltage at full state of charge	V	30
Voltage at zero state of charge	V	20
Energy	kWh	1.6

Table 3.2: Data of the lithium-ion battery at the low voltage side of the DC/DC converter.

3.5.2 Simulation

In order to simulate its presence, the DC/DC converter was represented as two current control sources, one of them connected to the model of the battery and the other injecting or extracting current from the DC-link with the appropriate transformer ratio. The drawback of this is that the switching effects can't be evaluated, but at least it allows a faster simulation. Anyway, the main objective of this part is checking if having something like this in the real design could provide an improvement in the control of the DC-link voltage.

A key point here is the relationship between both converters (1 and 3). The control had to be thought in such a way that individual controls of both converters don't fight over the regulation. The rectifier (converter 1) is the one that has to maintain the voltage in steady state. Only if there is a deviation of the reference, the DC/DC

converter should inject or extract current in order to balance the system in a faster way while complying with the regulation. With this, and since the rectifier control already includes a PI to guarantee zero error in steady state, the control of the current flowing in the battery could be done with a PD controller. The differential action would only work if the voltage error changed its value. This is shown in fig. 3-12.

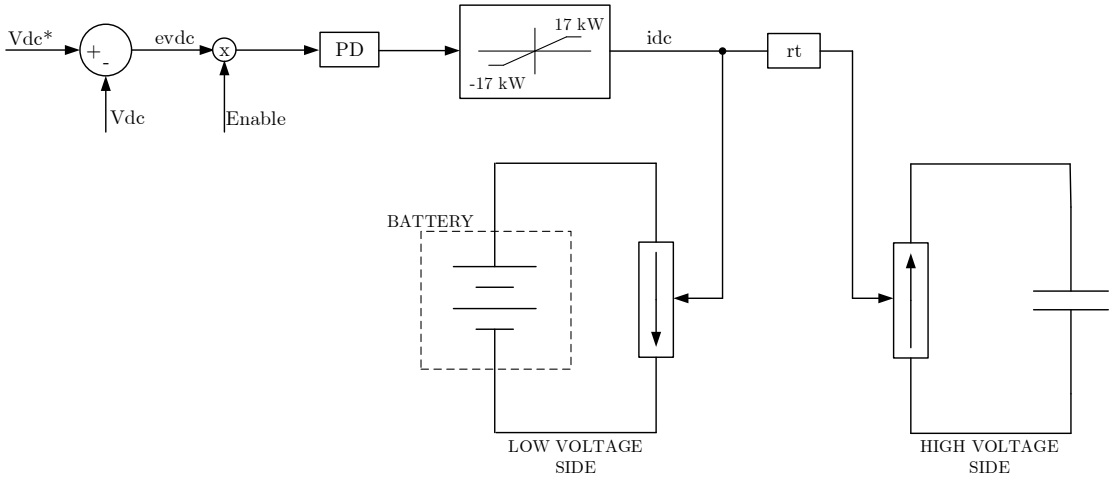

Figure 3-12: DC/DC converter scheme with the control loop. Rt represents the transformer's ratio between the high voltage side and the low voltage side.

The extra current flow provided by the DC/DC converter is calculated proportionally to the error until it reaches the limit imposed by the power. The differential action allows a faster response than just using the proportional action, as it will be shown in further sections. The enable port is added for several reasons:

- If the error is smaller than 2.5 V there won't be current flowing through the battery, as it will be considered as normal fluctuations in the voltage level. This way we avoid charging and discharging the battery unnecessarily.

- If the error is positive means the voltage in the capacitor is smaller than the reference, so there should be current injection in the capacitor, that will come out of the battery. If in this case the voltage in the battery is smaller than 20 V, there won't be current extraction because that would degrade the battery.

- Opposite to previous case, if the error is negative means the voltage in the DC-link is greater than the reference, so there should be a current extraction from the capacitor in order to lower the voltage. If the voltage in the battery is 30 V, there won't be current extraction allowance because that would also damage the battery.

Transformer's ratio is calculated dynamically as the voltage in the DC-link divided by the voltage in the battery. Current in the high voltage side of the converter is then computed as the current in the low voltage side divided by this transformer's ratio. The operation of this converter together with the other parts of the system is shown in section 3.7.

3.6 Load voltage control

In this section it is presented the control of the inverter connected to the AC loads. This 3-phase converter is in charge of controlling the voltage in the loads. This feature was tried independently, substituting the capacitor by an ideal voltage source of 600 V, as it can be seen in fig. 3-13.

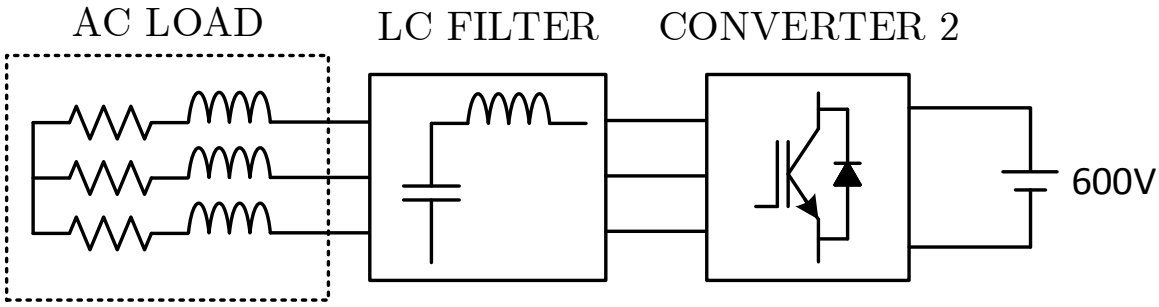

Figure 3-13: Scheme for AC load control from a DC voltage source.

At this point there were some problems regarding the maximum AC voltage that is possible to obtain from the 600 V DC-link. The idea is to create a normalized grid at the output, 400 V line to line RMS (327 V phase to neutral peak) and 50 Hz. According to [25], using classical modulation, the maximum voltage that can be obtained in phase to neutral peak is ±Vdc/2, which means using only a 86.6% of

the voltage available. In this case ±300 V phase to neutral peak. A solution to this is using homopolar voltage injection, shifting the 3 references by the same amount in such a way that the sum of the 3 are no longer zero but the homopolar voltage. This way, the maximum voltage that can be obtained in phase to neutral peak is $\pm \mathrm{Vdc}/\sqrt{3}$, 346 V, which is enough in this case. A drawback of this is that the harmonic components of the input and output current will increase [26]. Since this is not the main objective of this thesis, the simulations were carried out reducing the voltage command for the load to a value that could be reached with classical modulation.

3.6.1 Filter design

The company didn't have yet the data for the filter design, so one LC filter was calculated in order to have frequencies filtered beginning at 900 Hz. In order to do so, and using equation 3.19 of the frequency in an LC filter, the value of the capacitor was selected to be 30 μF. With those values of frequency and capacitor, inductor value is 1 mH.

$$\omega = 2\pi f = \frac{1}{\sqrt{L_f C_f}} \tag{3.19}$$

The parasitic resistor of the inductor was estimated at 0.05 Ω, because it is a filter for high power and otherwise the voltage drop in it will be unacceptable.

3.6.2 Control

As in section 3.2, the control will be realize with two nested loops, one for the current and one for the voltage, with an appropriate bandwidth separation. In this case, q-axis current will be forced to zero in such a way that all the voltage will be controlled with the d-axis, being the module of the reference equal to the d-axis voltage command.

3.6.2.1 Current control loop

The scheme is the same as in fig. 3-2. Both d and q axes loops are tuned as in 3.2.1, using zero-pole cancellation by means of the elements in the LC filter (the resistance used is the parasitic resistance in the inductance) with a bandwidth of 500 Hz. Cross-coupling terms are present too, with the difference that there is no BEMF term and the inductance is the same for both axis. For the dq to abc transformation, the synchronization is made with the grid voltage angle. As it was previously mentioned, the objective of this thesis is not the synchronization for the transformation, so it is considered that the voltage is a perfect sinusoidal waveform rotating at 50 Hz. If this is intended to be made more realistic, a Phase-Locked Loop (PLL) could be implemented in order to track it.

3.6.2.2 Voltage control loop

Voltage control loop is similar to the one in fig. 3-5, but this time in the d-axis. In the case of the PI, the tuning is done in the same way, using Sisotool with the value of the capacitor in the filter and a bandwidth of 40 Hz.

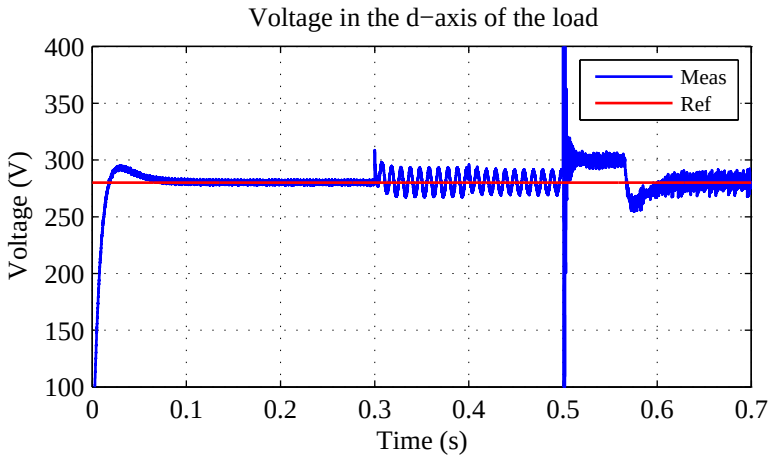

Figure 3-14: Voltage in d-axis at the load alongside its reference.

3.6.3 Simulation

Scheme from fig. 3-13 was implemented in Simulink in order to test the design of the loops. Voltage reference can't be 300 V because there is a voltage droop in the filter elements, so in order to have some margin the voltage command was set to 280 V.

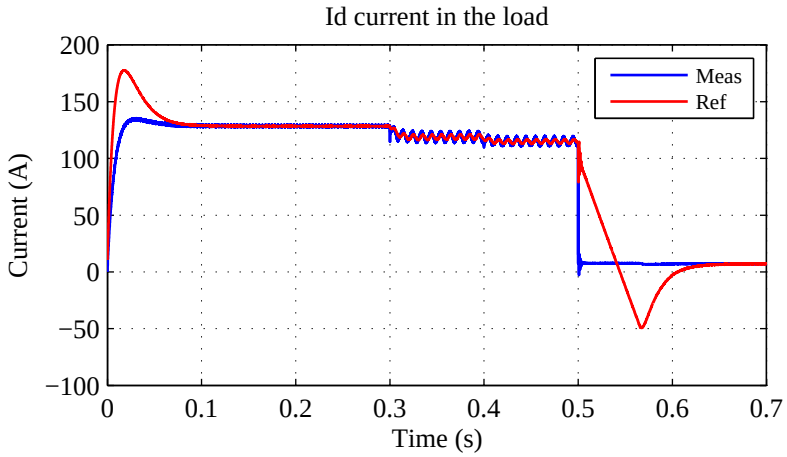

(a) Id

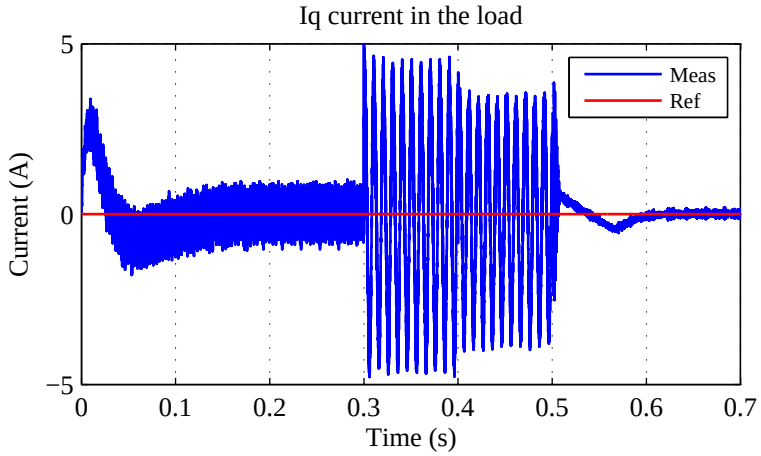

(b) Iq

Figure 3-15: Currents id(3-15a) and iq(3-15b) in the load when the voltage in the d-axis is controlled to be 250 V as peak phase to neutral.

The simulation works as explained below:

- **0 s:** Initially the load is balance, resistive and demanding 20 kW per phase.
- **0.3 s:** There is an unbalance of a 20% in phase 3.

- **0.4 s:** There is another unbalance of a 10% in phase 2, maintaining also the one in phase 3.

- **0.5 s:** The load goes back to being balance, but the demand is 1 kW per phase. This is a big step in the load.

In fig. 3-14 it can be seen how the voltage tracks the reference in the d-axis. From 0.3 to 0.5 seconds the resulting voltage is oscillating because of the imbalance.

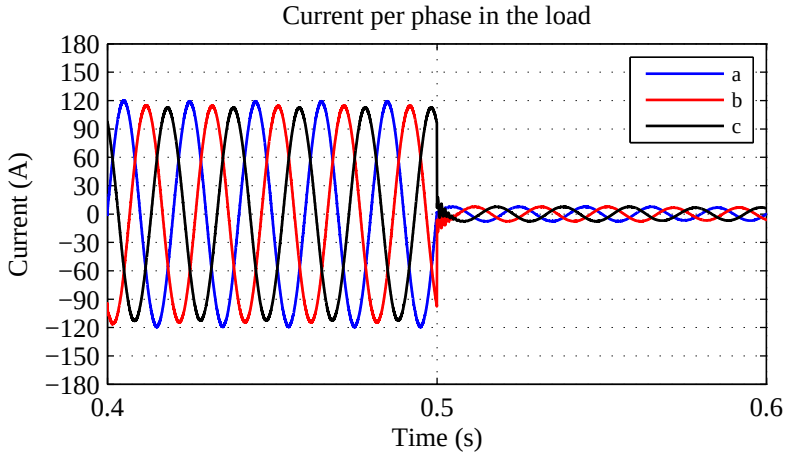

(a) Iabc

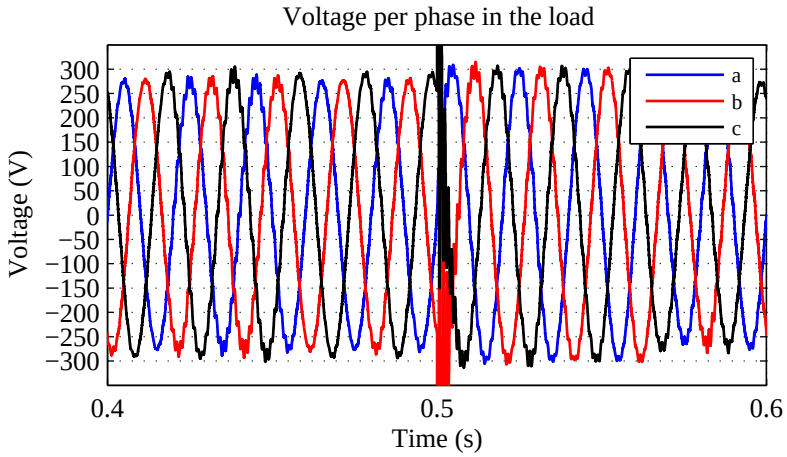

(b) Vabc

Figure 3-16: Currents (3-16a) and voltages (3-16b) per phase in abc coordinates in the load when the voltage in the d-axis is controlled to be 250 V as peak phase to neutral.

The inner current loops are also working properly, as seen from fig. 3-15 where both axes are following the reference much faster than the voltage loop (they were

designed with a higher bandwidth). Between 0.3 and 0.5 seconds the same ripple seen in the voltage level can be appreciate at the current level. From 0.5 seconds the current is dramatically reduced because of the power reduction. Finally, the currents and voltages in abc reference frame measured at the point of connection of the load with the filter are shown in fig. 3-16, phase to neutral quantities. In order to have a good view, only instants from 0.4 to 0.6 seconds are shown, to see the change in the power. They are displayed in order to demonstrate that the filter designed is working fine at filtering the voltage so it is sinusoidal at the load. Of course, the peak value in the voltage is the same as the d-axis voltage reference, since the q-axis is controlled to be zero (with the current) and all the module is reflected in the first axis.

3.7 Integration of all the systems

Once all the systems were presented and tested individually, everything was put together as in the scheme from fig. 1-3. In this section the simulation results in the DC-link are presented for different cases: system working without DC/DC, using the DC/DC and just a proportional action for its control and using the DC/DC with the PD controller. The aim of this is to show the improvements that the DC/DC correctly controlled can bring in to the stabilization of the DC-link voltage.

In order to do so, a simulation was prepared to last 0.8 seconds. The speed in the PMSM is set to 5500 rpm and the DC-link voltage reference to 600 V as always. The simulation works as the one in the previous section (starting with 18 kW per phase and having all the changes being the same).

The different load states were prepared to see the changes in the DC-link and compared the best option. This states vary really fast and the load changes are very sharp, which is not expected normally, but it is done in this way in order to have a better comparison. The 3 different cases are presented in fig. 3-17.

There are several remarkable aspects that are clear from the graph. One is that all the methods are complying with the regulations in this case: the voltage is always between the pink limits and there is never a ripple bigger than 9 V. In the base case

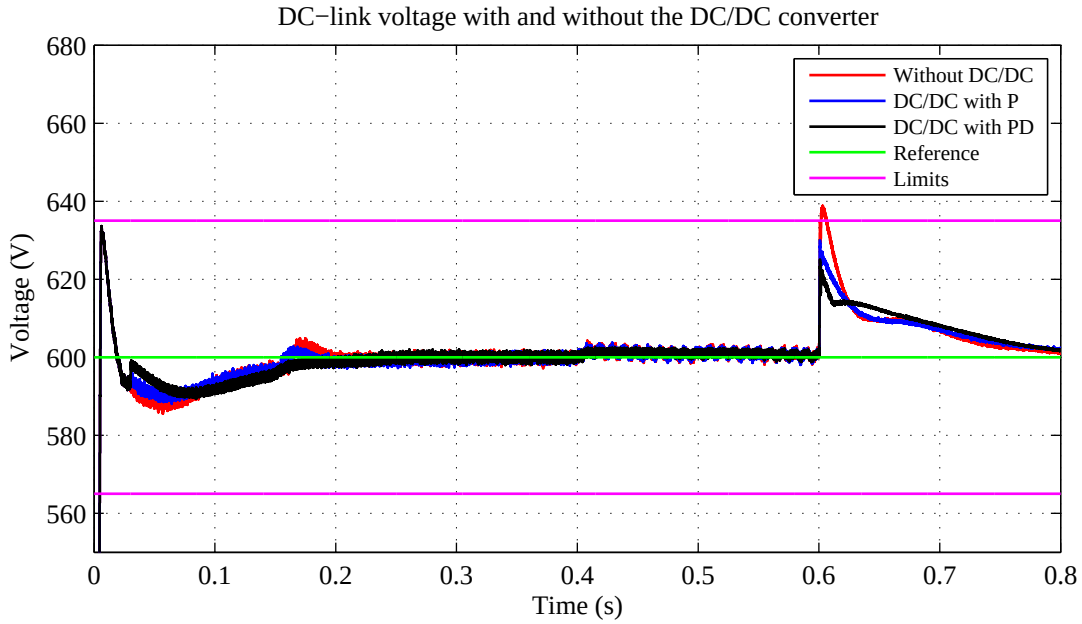

Figure 3-17: Voltage in the DC-link in different situations: when there is no DC/DC converter, when the DC/DC converter is controlled with a proportional action and when it is controlled with a PD controller.

without DC/DC converter there is a peak over the upper limit when the load changes sharply to a small value (around 0.6 seconds), but the time it lasts is between the limits of normals transients as seen from fig. 3-6.

The other aspect is that the best option is to control the DC/DC converter with a PD regulator, even when just adding the DC/DC converter with the additional power of the battery causes an improvement in the system's general performance.

3.8 DC-link voltage variations reduction

Once all the subsystems are connected and working together it came the time to try some reduction methods.

3.8.1 Including an extra power source

This refers to the use of the DC/DC converter. As it has been shown in previous section (fig. 3-17), this converter leads a very positive effect when it has to stabilize

the DC-bus voltage, and it is really appealing during transients.

3.8.2 Feedforward current term

One of the most interesting methods found during the research carried out about the methods for reducing the DC-link capacitor was the use of the feedforward terms [7–9,17]. It is also one of the easiest methods that can be implemented once the whole simulation is completed. The working principle was already explained in chapter 2. In here it will be used as follows: the voltage control loop for the voltage at the load generates a current command in the d-axis. In parallel, there is a loop controlling the DC-link voltage. If there is a power change without any coupling between loops, what happens first is that the load loop starts extracting/injecting current from/in the capacitor, and the other loops reacts to this when the voltage starts changing, with a delay. What it is proposed here is to use the current command generated in the load loop (d-axis) and add it to the current command in the other loop (q-axis). This way, the controller already knows there is a new demand in the system and anticipates the current change, in such a way that it comes from the generator and not from the capacitor, producing a smaller variation in the voltage. Obviously, a small variation is unavoidable because there are still some delays in the loops and communications. The biggest drawback of this is the need of fast communication between converters controllers. The fastest the communications, the smaller the delay and the smaller the variation in the DC-link voltage [8].

It is important to note that the feedforward term can't be directly added to the current command in the DC-link loop because they are not based in the same voltage. Current has to be transformed using power balance and assuming no power losses between converters, as it was done in section 3.2.2, but this time using the power in dq coordinates in the load, as shown in eq. 3.20. The term 3/2 in the power is because the abc to dq transformation performance is not power conservative.

$$P_{DC} = P_{AC} = V_{DC} I_{DC}^{*} = \frac{3}{2}(V_d i_d + V_q i_q) \tag{3.20}$$

The voltage in the DC-link when a feedforward term is added is shown in fig. 3-18 (same power changes as in previous section). Different scenarios were tried out. The base case without DC/DC is compared with the case without DC/DC but feedforward term and the case of a DC/DC controlled with a proportional action alone or a PD controller. As it is expected, the best case is the one including the PD controller for the DC/DC and the feedforward term for the currents (pink curve).

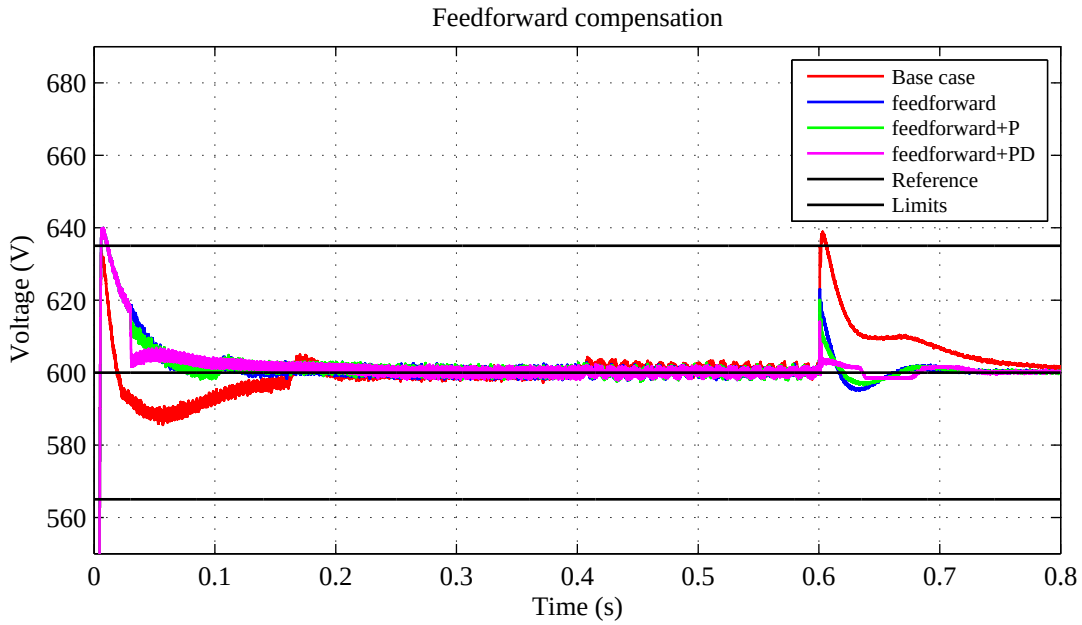

Figure 3-18: Voltage in the DC-link when there is a feedforward compensator in the current loop.

3.8.2.1 Delay effects

As it was previously mentioned, when using feedforward there is a need of fast communications between the different units in the system. A typical protocol for doing the communications in a car (independently of its type) is the CAN (Controller Area Network); a multi-master, message broadcast system developed by BOSCH. All the buses in the system work at the same speed, which can be selected from a wide range as indicates the standard for this protocol [27]. In this case, all the modules are connected with a CAN bus with a baudrate of 125 kbps. This speed is the maximum that it can be achieved in what is called "fault tolerant CAN bus". Its main benefit

is that it can operate under different failures, analysing continuously the bus in order to return to normal operation if the fault disappears. In the worst case, and using eq. 3.21, the time delay could be around 1264 μs [28, 29].

$$T = 44 + 8 \cdot DLC + \frac{34 + 8 \cdot DLC}{4} \cdot T_{bit} \tag{3.21}$$

Where DLC is data length (between 1 and 8 bytes) and T_{bit} is the bit time. If this delay is applied to previous simulations it can be compared how worse the system performance becomes. This is shown in fig. 3-19. In order to see it better just 0.1 seconds are shown. As it can be seen, even the worst delay at that speed does not really spoil the behaviour and still compensates for the extra communications. This means that in other more favourable cases the difference will be smaller, which is a good reason to choose this method.

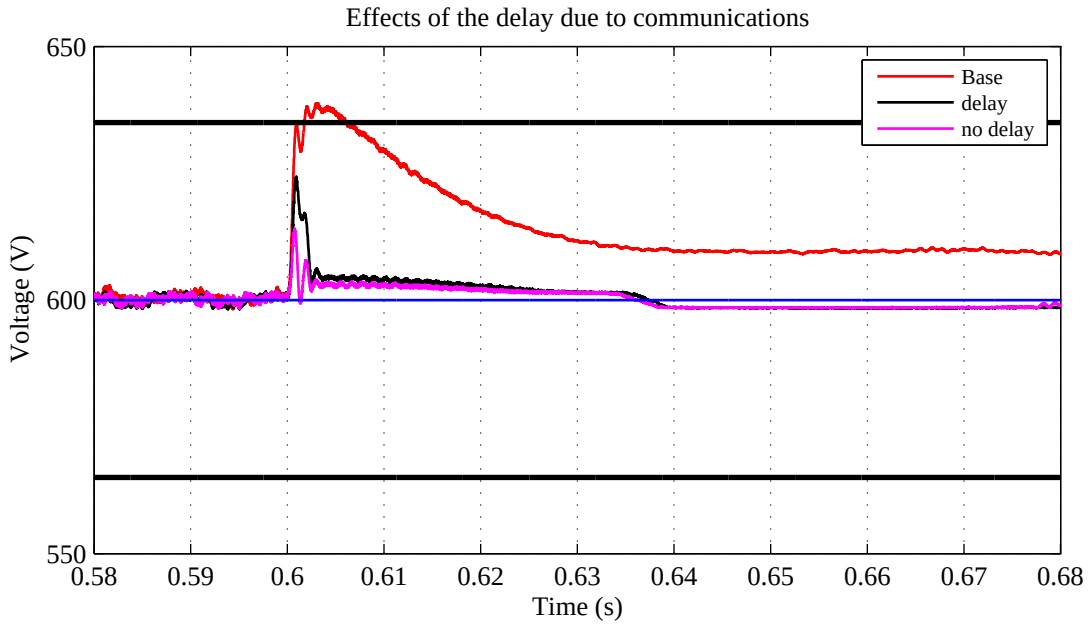

Figure 3-19: Voltage in the DC-link when there is a feedforward compensator in the current loop and there are delays in the communications compared to the case where there are no delays and the base case.

3.8.2.2 Effects of reducing the capacitor

In this section it has been demonstrated how adding feedforward current from the load helps a lot stabilizing the bus, which means an smaller capacitor could be employed. Previous simulation has been repeated reducing the capacitor from 2 mF to 0.5 mF. The results are displayed for the base case, the use of a DC/DC and the use of a DC/DC in addition to the feedforward term.

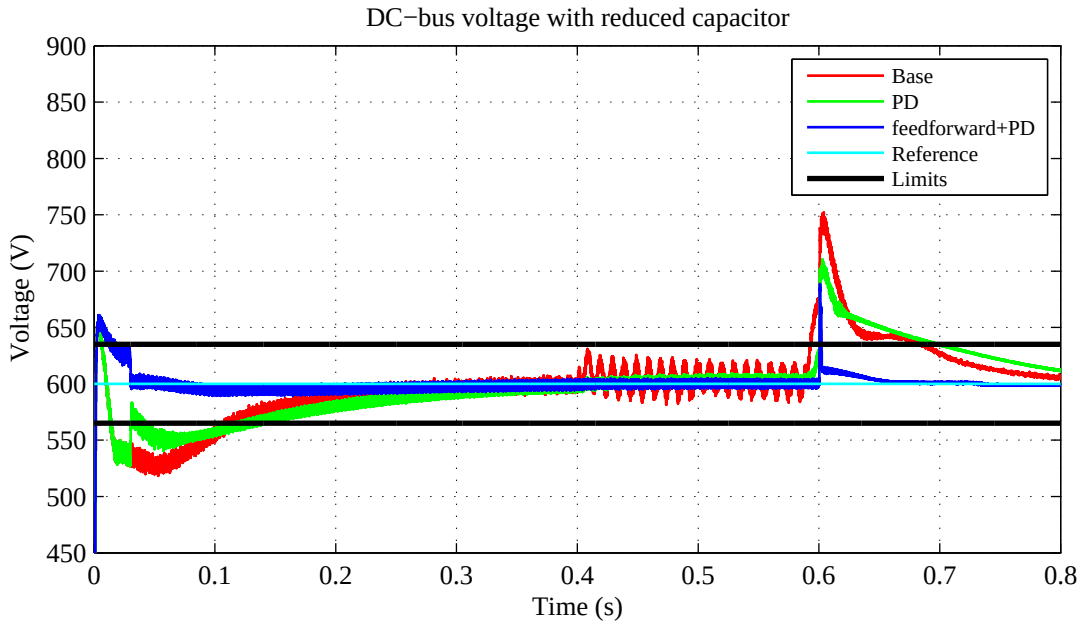

Figure 3-20: Voltage in the DC-link when the capacitor is reduced from 2 mF to 0.5 mF.

With this capacitor, the only curve complying with the normative is the blue curve, the one extracted from the voltage simulation using feedforward.

Chapter 4

Conclusions and future work

4.1 Conclusions

The most important part of this work was the analysis of the state of the art in the topic of potential actions that can be carried out in order to minimize the capacitor in the DC-link in a power electronics configuration for transport applications. It consist of an extensive research about the topic, being the main interest of the company for whom this thesis was carried out. The different methods were classified between three different groups: modification of the inverter topology, power balance control and modification of the PWM modulation scheme.

Once this classification was done, the initial idea of the company, using a 2 mF capacitor was studied. In order to do so, the system presented in fig. 1-3 was represented in Matlab Simulink. One of the most important simplifications here was the fact that the DC/DC converter was modelled as a non-switching converter, using controlled current sources. This was done in order to achieve faster simulations but also because the final converter was still not developed by the company. Simulation results showed that the system performance is loosely between the limits with this capacitor, so it is possible to look for smaller and cheaper capacitors. It has been demonstrate that the use of the converter improves the system performance, which was one objective of this thesis. In addition to this, the use of a feedforward current term has show the potential to further reduce the voltage variations, allowing an even

bigger capacitor reduction.

4.2 Future work

This is not the end of the project. Some future work that is going to be carried out includes:

- Test some methods that were mentioned in the chapter regarding the state of the art that weren't tried yet.
- Continuous update of the existing methods by getting all new publications.
- Set an experimental mounting in order to try the methods in real life, so Simulink results are validated.

Appendix A

DQ Synchronous Reference Frame

As for this thesis, rotating vectors will be used (also known as space vectors), because of the simplicity they bring and also because they transform 3-phase variables into two, allowing a better performance in the control and zero steady state errors when using PI controllers. Phase currents normally add up to zero, which means that there are really only two independent variables. If there were 3 controllers, one for each variable in abc coordinates, they would "fight" over the regulation. If vectors are in an arbitrary reference frame, signals are still changing in steady state, so the reference frame is made to rotate at the same speed as the complex vector, having finally constant signals at steady state with a consequent zero error when using a PI [30].

Transformation abc to dq is done thanks to eq. A.1, where f represents any abc quantity, and the constant (2/3) allows the transformation to be conservative with respect to the amplitude, but not respect to the power (power calculations must take this into account). This is known as the Park transformation.

$$\bar{f_{qd}} = \frac{2}{3}\Big(f_a + f_b e^{j\frac{2\pi}{3}} + f_c e^{j\frac{4\pi}{3}}\Big) = \frac{2}{3}\Big(f_a + a f_b + a^2 f_c\Big) \tag{A.1}$$

Projecting the space vector on the d (direct) and q (quadrature) axes gives the components d and q of this complex vector. This rotating vector describes a 3-phase system, and it is not a phasor. Particularly, if a 3-phase system is symmetrical with

pulsation ω_e, the space vector generated will have constant amplitude and it will rotate at an angular speed of ω_e.

Appendix B

Sine-triangle modulation

The idea of sine-triangle PWM is generating gate command for the different switches in a converter by comparing the references in abc coordinates with a triangular waveform that has as frequency the desired switching frequency, as shown in fig. B-1. In this image, the switching frequency has being reduced for convenience and clarity.

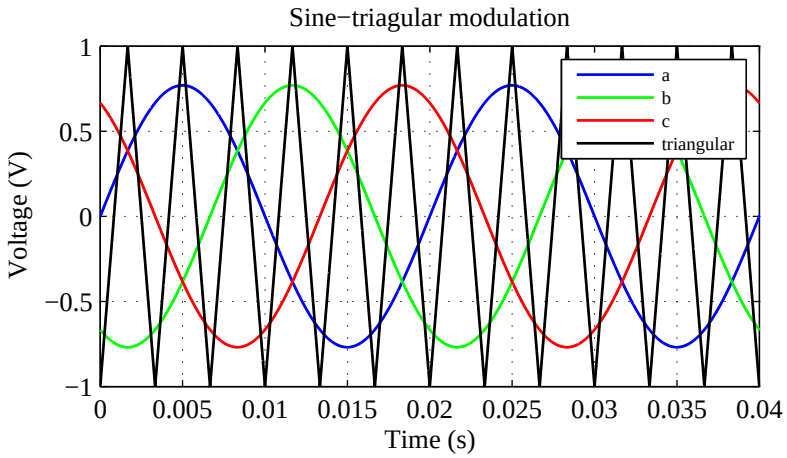

Figure B-1: Example of sinusoidal references compared to a triangular carrier. The frequency of the carrier has being diminish in order to visualize the idea correctly.

The triangular carrier, which is the same for the 3 references, is compared with the sinusoidal waveform, generating an square waveform. This is the command for the upper switch in a branch, being the opposite for the lower one. This is shown in fig. B-2. If the switching frequency is high enough compared with the fundamental frequency, in a switching period the references can be considered to be straight.

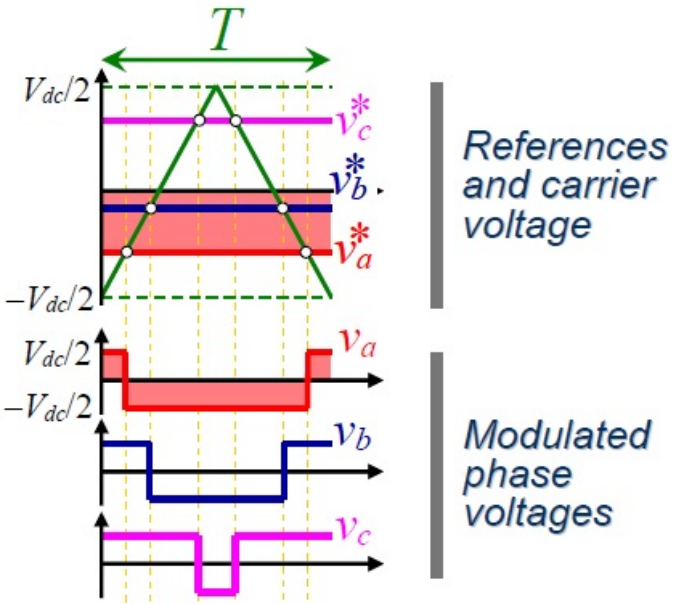

Figure B-2: References and carriers in one switching period, and the square waveforms generated [25].

As a final comment, overmodulation occurs when one of the references touches the peak, moment in which the maximum voltage available with this classic method is reached.

Bibliography

[1] BP Global, "BP statistical review of world energy," June 2015.

[2] United States Environmental Protection Agency (EPA), "Overview of greenhouse gases," 2016.

[3] National Aeronautics and Space Administration (NASA), "GISS surface temperature analysis," 2016.

[4] L. Wilson, "Shades of green: Electric cars' carbon emissions around the globe," 2013.

[5] J. Liu, H. Wen, and X. Zhang, "Analysis of the vsi with small DC-link capacitor for electric vehicles," in *Electrical Machines and Systems, 2008. ICEMS 2008. International Conference on*, pp. 1401–1405, Oct 2008.

[6] H. Ye and A. Emadi, "An interleaving scheme to reduce DC-link current harmonics of dual traction inverters in hybrid electric vehicles," in *2014 IEEE Applied Power Electronics Conference and Exposition - APEC 2014*, pp. 3205–3211, March 2014.

[7] L. Malesani, L. Rossetto, P. Tenti, and P. Tomasin, "AC/DC/AC PWM converter with reduced energy storage in the DC link," *IEEE Transactions on Industry Applications*, vol. 31, pp. 287–292, Mar 1995.

[8] B. gwan Gu and K. Nam, "A DC link capacitor minimization method through direct capacitor current control," in *Industry Applications Conference, 2002. 37th IAS Annual Meeting. Conference Record of the*, vol. 2, pp. 811–817 vol.2, Oct 2002.

[9] J. Jung, S. Lim, and K. Nam, "A feedback linearizing control scheme for a PWM converter-inverter having a very small DC-link capacitor," *IEEE Transactions on Industry Applications*, vol. 35, pp. 1124–1131, Sep 1999.

[10] W. J. Lee and S. K. Sul, "DC-link voltage stabilization for reduced DC-link capacitor inverter," in *2009 IEEE Energy Conversion Congress and Exposition*, pp. 1740–1744, Sept 2009.

[11] X. Lu, W. Qian, D. Cao, F. Z. Peng, and J. Liu, "A carrier modulation method for minimizing the DC link capacitor current ripple of the HEV DC-DC converter and inverter systems," in *Applied Power Electronics Conference and Exposition (APEC), 2011 Twenty-Sixth Annual IEEE*, pp. 800–807, March 2011.

[12] X. Lu and F. Z. Peng, "Theoretical analysis of DC link capacitor current ripple reduction in the HEV DC-DC converter and inverter system using a carrier modulation method," in *2012 IEEE Energy Conversion Congress and Exposition (ECCE)*, pp. 2833–2839, Sept 2012.

[13] J. Hobraiche, J. P. Vilain, P. Macret, and N. Patin, "A new PWM strategy to reduce the inverter input current ripples," *IEEE Transactions on Power Electronics*, vol. 24, pp. 172–180, Jan 2009.

[14] T. D. Nguyen, N. Patin, and G. Friedrich, "A PWM strategy dedicated to RMS current reduction in DC link capacitor of an embedded three phase inverter," in *Power Electronics and Applications (EPE 2011), Proceedings of the 2011-14th European Conference on*, pp. 1–9, Aug 2011.

[15] T. D. Nguyen, N. Patin, and G. Friedrich, "PWM strategy dedicated to the reduction of DC bus capacitor stress in embedded three phase inverter," in *2011 IEEE Vehicle Power and Propulsion Conference*, pp. 1–6, Sept 2011.

[16] T. D. Nguyen, N. Patin, and G. Friedrich, "Extended double carrier PWM strategy dedicated to RMS current reduction in DC link capacitors of three-phase inverters," *IEEE Transactions on Power Electronics*, vol. 29, pp. 396–406, Jan 2014.

[17] C.-C. Hou and H.-P. Su, "A multi-carrier PWM for AC-DC-AC converter without DC link electrolytic capacitor," in *2014 International Power Electronics Conference (IPEC-Hiroshima 2014 - ECCE ASIA)*, pp. 2821–2825, May 2014.

[18] A. Fratta, P. Guglielmi, G. M. Pellegrino, and F. Villata, "DC-AC conversion strategy optimized for battery or fuel-cell-supplied AC motor drives," in *Industrial Electronics, 2000. ISIE 2000. Proceedings of the 2000 IEEE International Symposium on*, vol. 1, pp. 230–235 vol.1, 2000.

[19] C. Sommer, A. Merkert, and A. Mertens, "A new control method for minimizing the DC-link capacitor current of HEV inverter systems," in *2014 IEEE Energy Conversion Congress and Exposition (ECCE)*, pp. 1188–1193, Sept 2014.

[20] A. Cimpoeru, *Encoderless Vector Control of PMSG for Wind Turbine Applications*. PhD thesis, University of Aalborg, Denmark, 2010.

[21] F. G. Capponi, *Lecture notes in Dynamic Analysis and Control of AC machines*. Sapienza: Università di Roma, 2014.

[22] R. Bojoi and E. Armando, "Getting the Back-Emf Voltage Constant of Permanent Magnet Motors with Just one Twist of the Wrist using Gen3i Data Recorder," in *HBM. Measure and predict with confidence*, 2016.

[23] B. Akin and M. Bhardwaj, *Application note on Sensored Field Oriented Control of 3-Phase Permanent Magnet Synchronous Motors.* Texas Instruments, 1.1 ed., Feb 2010.

[24] Detroit. Demand Performance, *The Detroit DD15 Engine. Takes innovation to a whole new level*, 2016.

[25] F. B. del Blanco, *Lecture notes in Dynamic Analysis and Control of AC machines.* Escuela Politécnica de Ingenería de Gijón: Universidad de Oviedo, 2014.

[26] M. E. de Oliveira Filho, J. R. Gazoli, A. J. S. Filho, and E. R. Filho, "A control method for voltage source inverter without dc link capacitor," in *2008 IEEE Power Electronics Specialists Conference*, pp. 4432–4437, June 2008.

[27] S. Corrigan, *Application report on Introduction to the Controller Area Network (CAN).* Texas Instruments, July 2008.

[28] Embedded Systems Academy. Products, Consulting and Training for Embedded Systems, *CAN Best and Worst Case Calculator.*

[29] F. Schade and M. Muth, *Application note on Fault-tolerant CAN transceiver.* Application Hints, 1.5 ed., Feb 2016.

[30] T. A. Lipo, *Analysis of Synchronous Machines.* Wisconsin, USA: CRC Press, 2012.